

Spread of white-nose syndrome on a network regulated by geography and climate

Sean P. Maher*

Andrew M. Kramer

J. Tomlin Pulliam

Marcus A. Zokan

Sarah E. Bowden

Heather D. Barton#

Krisztian Magori+

John M. Drake

Author affiliations

Odum School of Ecology, University of Georgia, Athens GA 30602-2202

Current Address

*Museum of Vertebrate Zoology, University of California, Berkeley, Berkeley, CA 94720

#Department of Biology, Grove City College, Grove City, PA 16127

+School of Forestry and Wildlife Sciences, Auburn University, Auburn, AL 36849

Corresponding author:

Sean P. Maher

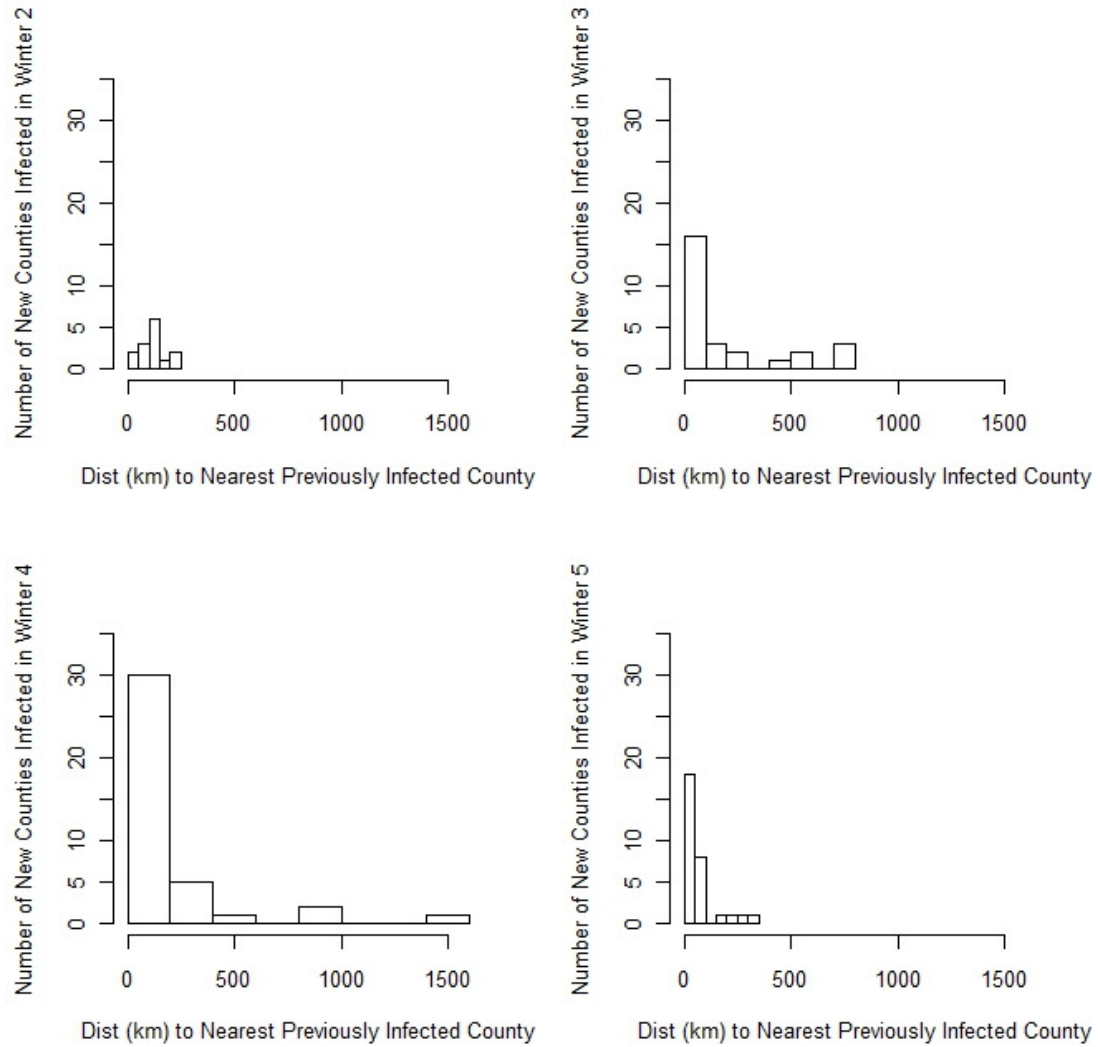
smaher02@gmail.com

Supplementary Information

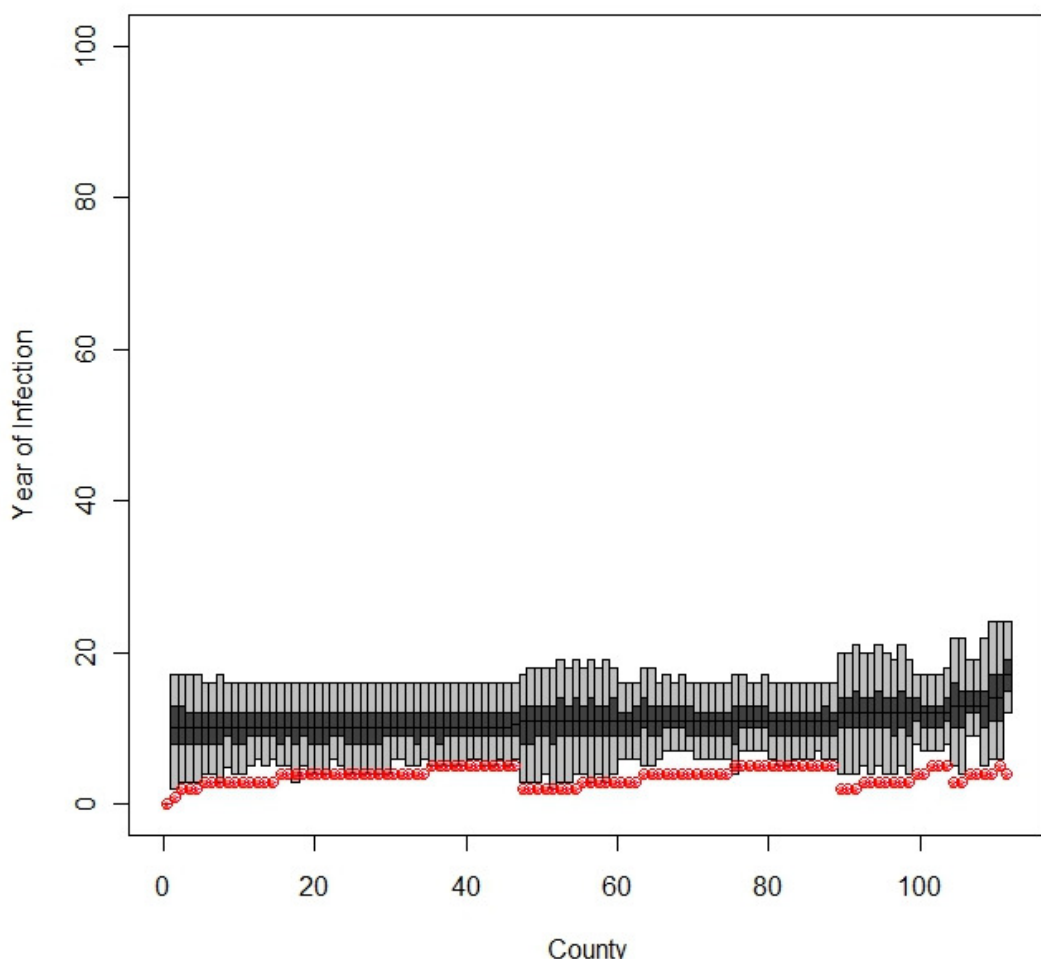
This supporting material provides details about data collection, model formulation and parameter estimation. Comprehensive results for all models are presented in table and figure format.

Table of Contents

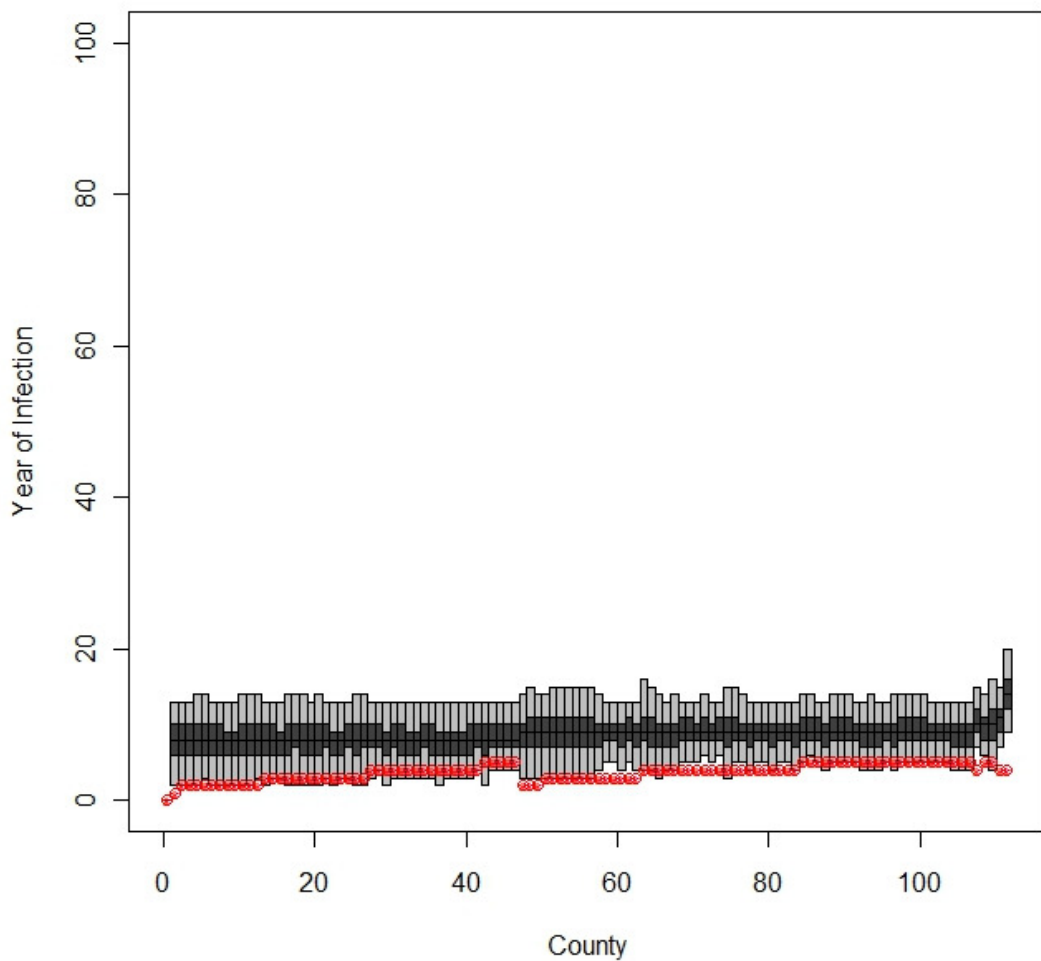
Observed “jump” plots (Supplementary Fig. S1)	Page 1
Summary plots of spatial spread characteristics (Supplementary Figs. S2–S27)	Pages 2–27
Imperfection detection plot (Supplementary Fig. S28).....	Pages 28–29
Geographic spread maps for gravity (caves) + winter model (Supplementary Figs. S29–S33)	
.....	Pages 30–34
Climate change scenario results (Supplementary Figs. S34–S44).....	Pages 35–45
Raw data figures and maps (Supplementary Figs. S45–S50)	Pages 46–51
Sample dispersal kernel plots (Supplementary Figs. S51–S53)	Pages 52–54
Tables (Supplementary Tables. S1–S6)	Pages 55–60
Habitat data description	Pages 61–62
Climate change data.....	Page 62
Calculation of probabilities.....	Page 62
Description of additional models	Pages 62–63
Dispersal kernel equations	Pages 63–69
Parameter estimation.....	Page 69–70
Simulation of spread	Page 70
Supplementary References.....	Page 71



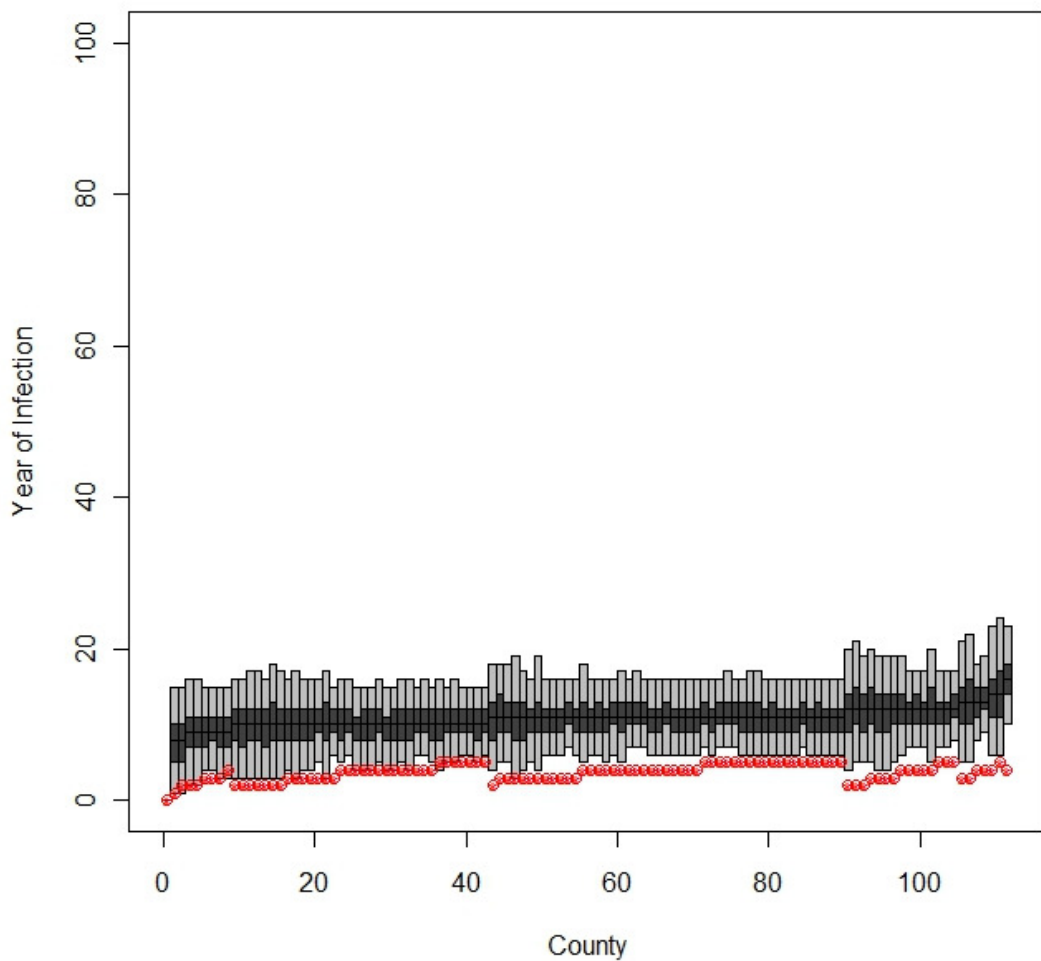
Supplementary Figure S1. Histograms of newly infected counties and the distance to the nearest previously infected county. Large “jumps” are seen in Winter 4, representing Woodward County in Oklahoma and Pike and Shannon Counties in Missouri. The long dispersal events in Winter 3 are 3 counties in Virginia (Smyth, Bland, and Giles). In Winters 2 and 5, most new infections were within 500km of a previously observed instance of White Nose Syndrome or *Geomyces destructans*.



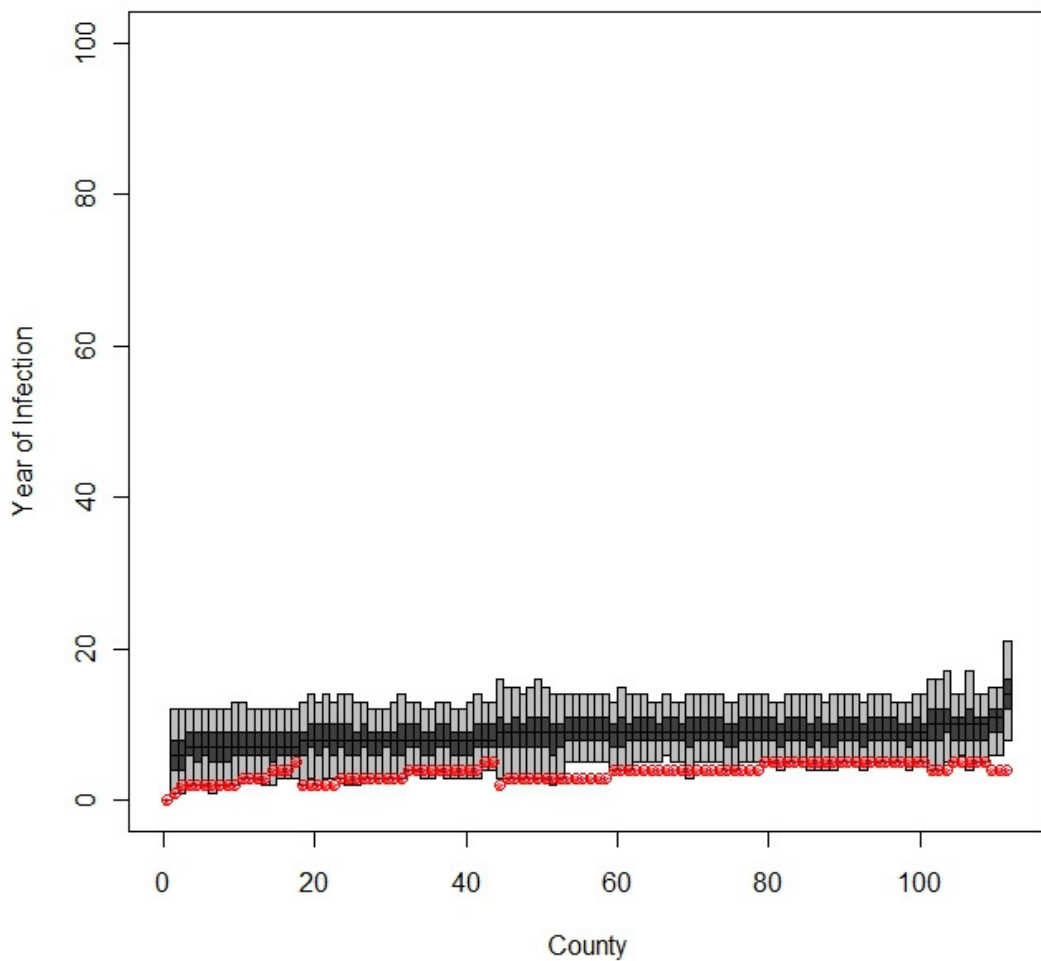
Supplementary Figure S2. The predicted year of infection for the currently (2010–2011) observed infected counties based on simulations from Schoharie County using the simple diffusion model for the contiguous United States under the ML parameter set. For each county, the 95% confidence range is in grey with the interquartile range specified by dark grey, with the simulated mean infection year as a black bar; red dots represent the observed year of infection for that county. Counties are ordered by the simulated year of infection. The model was able to estimate the given year of infection for a small subset of counties (26 of 112 counties).



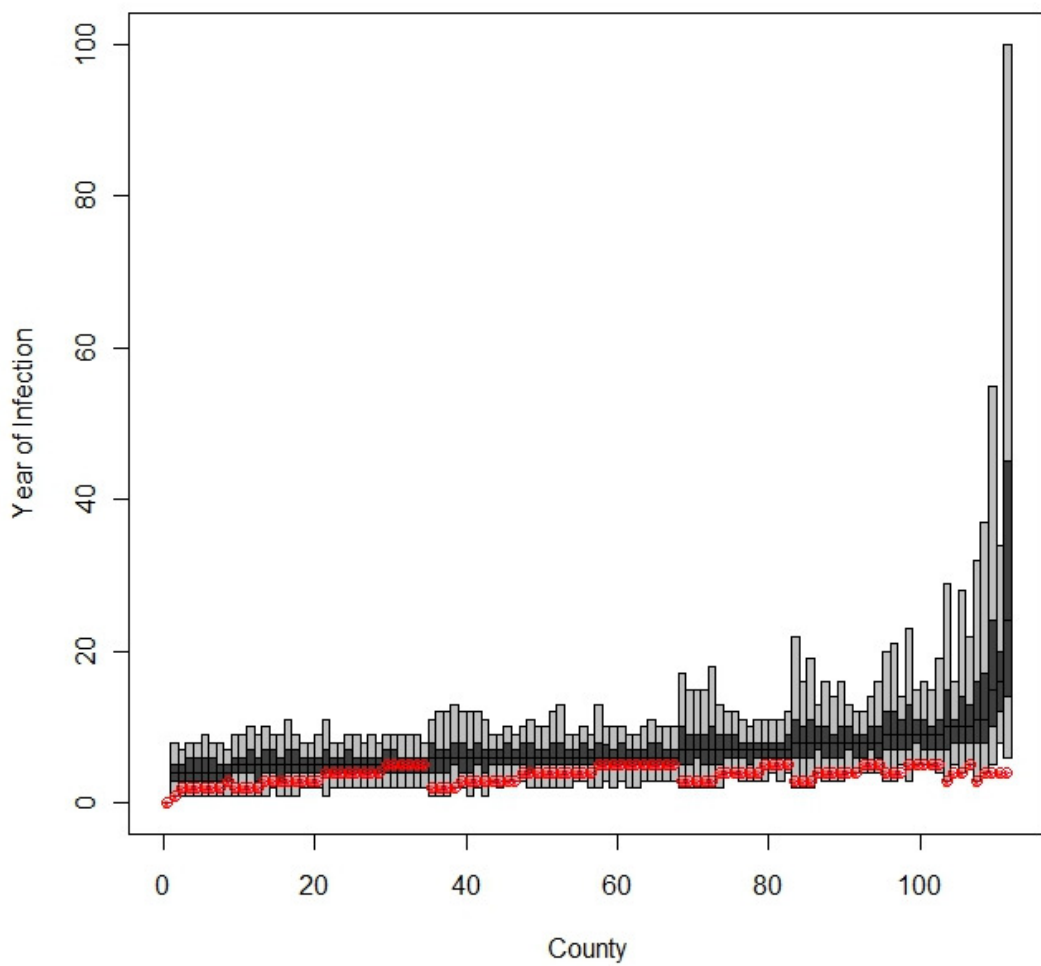
Supplementary Figure S3. The predicted year of infection for the currently (2010–2011) observed infected counties based on simulations from Schoharie County using the simple diffusion model constrained to counties with caves under the ML parameter set. For each county, the 95% confidence range is in grey with the interquartile range specified by dark grey, with the simulated mean infection year as a black bar; red dots represent the observed year of infection for that county. Counties are ordered by the simulated year of infection. The model was able to estimate the given year of infection for the majority of counties (83 of 112 counties).



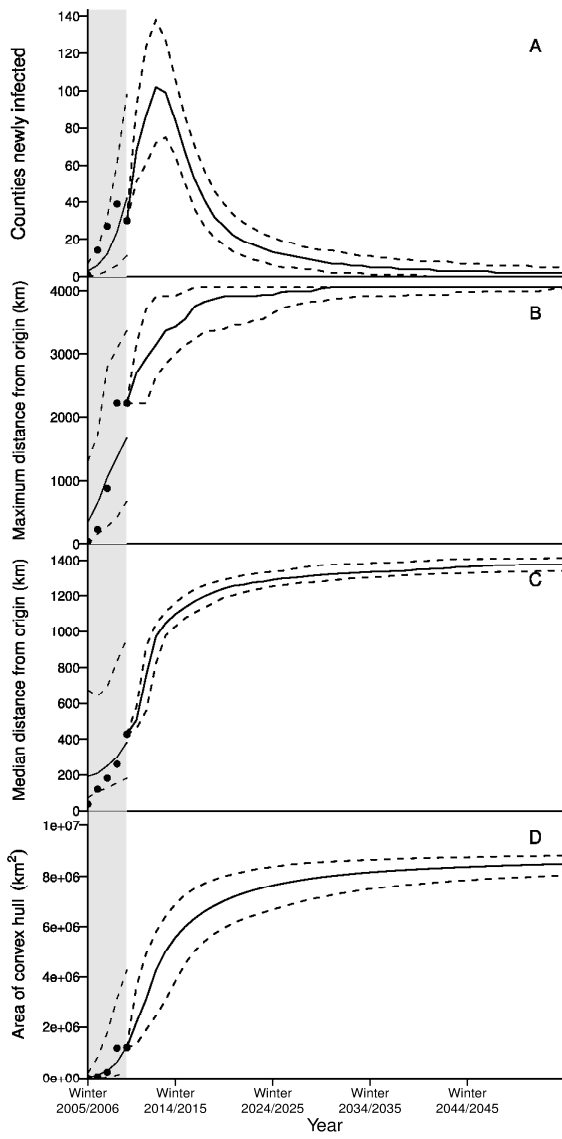
Supplementary Figure S4. The predicted year of infection for the currently (2010–2011) observed infected counties based on simulations from Schoharie County using the simple diffusion with long-distance dispersal model for the contiguous United States under the ML parameter set. For each county, the 95% confidence range is in grey with the interquartile range specified by dark grey, with the simulated mean infection year as a black bar; red dots represent the observed year of infection for that county. Counties are ordered by the simulated year of infection. The model was able to estimate the given year of infection for a small subset of counties (20 of 112 counties).



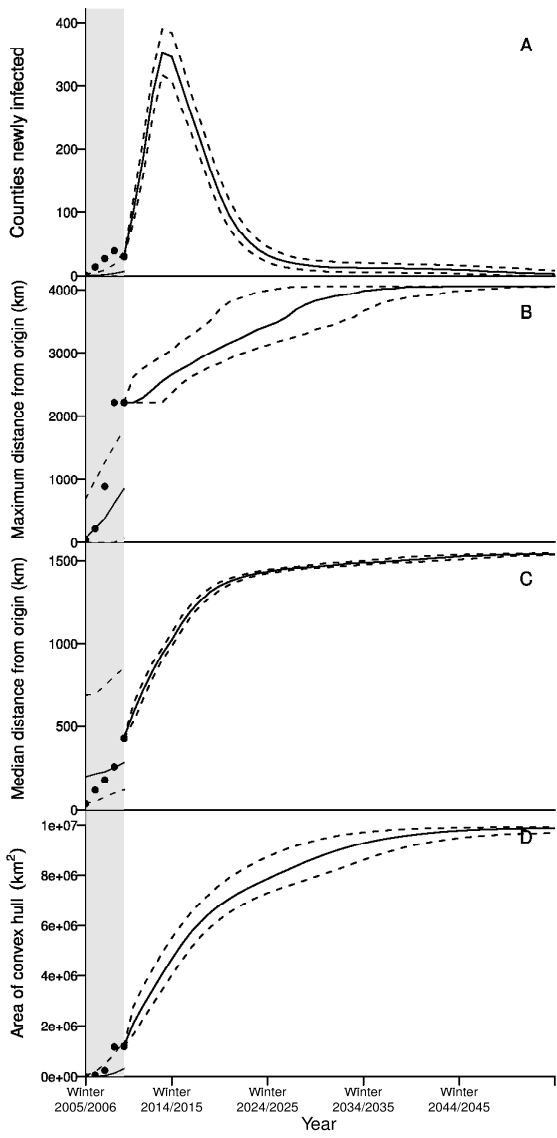
Supplementary Figure S5. The predicted year of infection for the currently (2010–2011) observed infected counties based on simulations from Schoharie County using the simple diffusion with long-distance dispersal model constrained to counties with caves under the ML parameter set. For each county, the 95% confidence range is in grey with the interquartile range specified by dark grey, with the simulated mean infection year as a black bar; red dots represent the observed year of infection for that county. Counties are ordered by the simulated year of infection. The model was able to estimate the given year of infection for the majority of counties (83 of 112 counties).



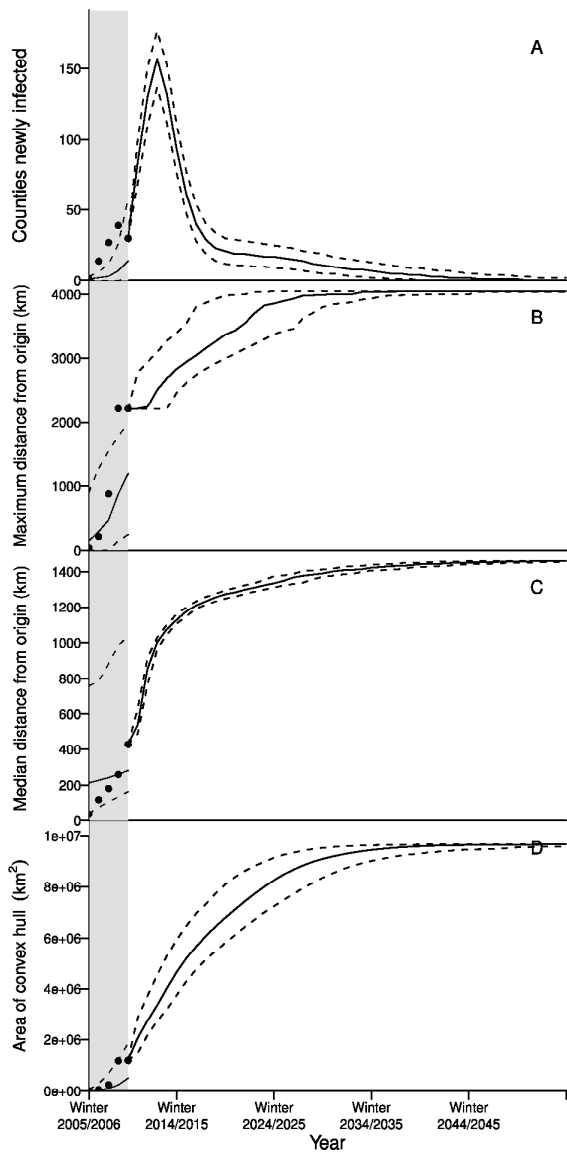
Supplementary Figure S6. The predicted year of infection for the currently (2010–2011) observed infected counties based on simulations from Schoharie County using the gravity_{caves+winter} model and the SU parameters. For each county, the 95% confidence range is in grey with the interquartile range specified by dark grey, with the simulated mean infection year as a black bar; red dots represent the observed year of infection for that county. Counties are ordered by the simulated year of infection. The model was able to estimate the given year of infection for a small subset of counties (26 of 112 counties).



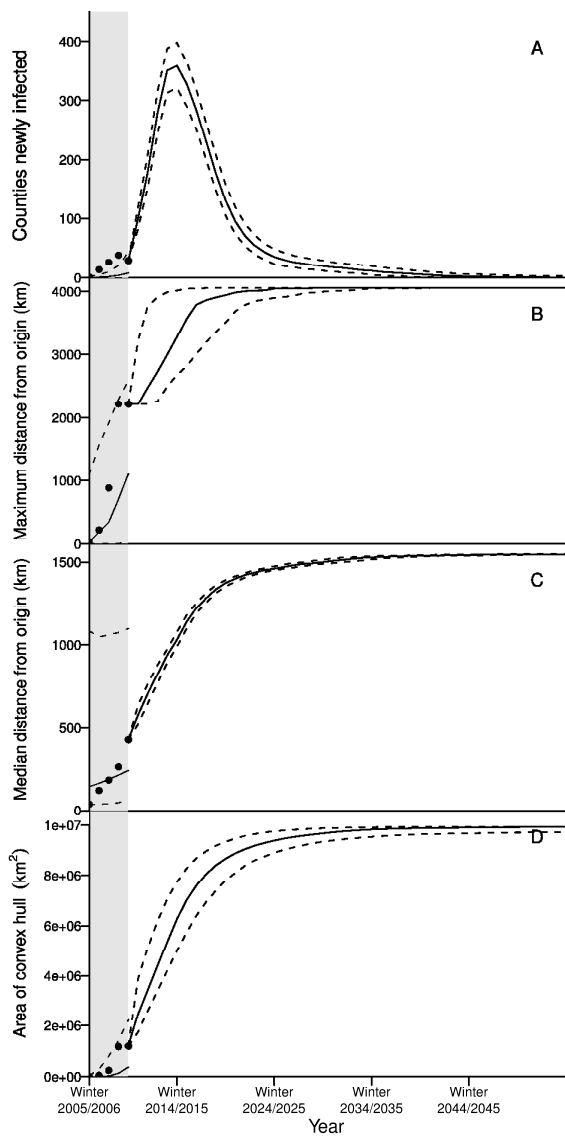
Supplementary Figure S7. Spread statistics for WNS based on the gravity_{caves}+winter model SU parameter set. Grey shading represents simulated spread from the Schoharie County, NY, and unshaded represents the results simulating from current (2010–2011) observations. Solid lines are median values and dotted lines represent 95% predictive interval. (A) The number of newly infected counties in the given winter, spread peaks in the winter of 2013–2014, and infection rate is consistent with observations in the first 5 winters of spread. (B and C) The maximum (B) and median (C) distance from Schoharie County, maximum distance from the origin will not be complete until the winter of 2031–2032. (D) The convex hull of infection area is the total area within the minimum convex polygon of infected county centroids.



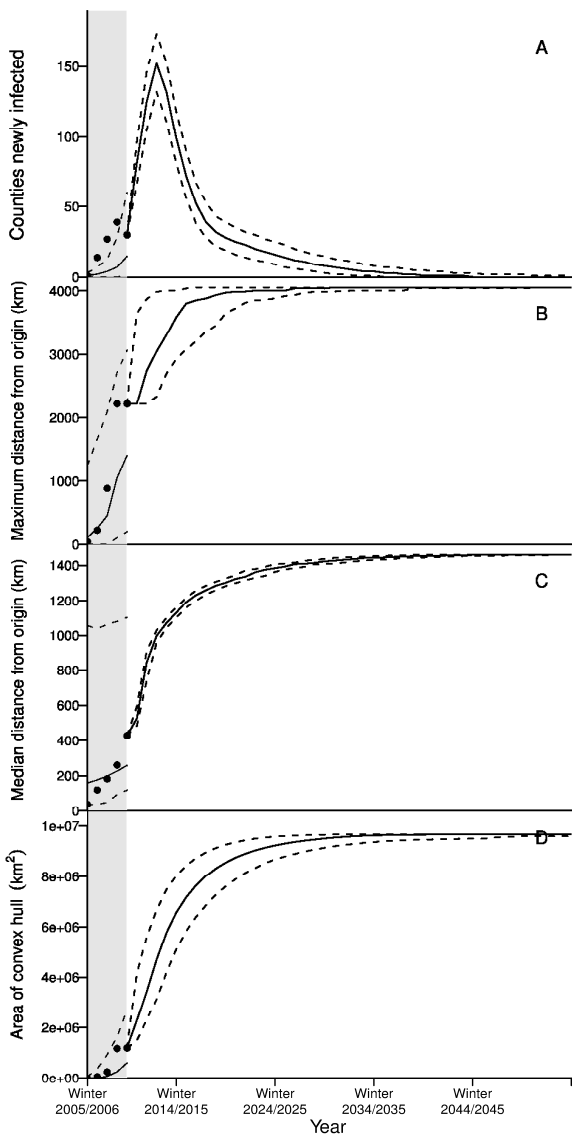
Supplementary Figure S8. Spread statistics for WNS based on the simple diffusion model for the contiguous United States ML parameter set. Grey shading represents simulated spread from the Schoharie County, NY, and unshaded represents the results simulating from current (2010–2011) observations. Solid lines are median values and dotted lines represent 95% predictive interval. (A) The number of newly infected counties in the given winter, spread peaks in the winter of 2014–2015, although infection rate is not consistent with observations in the first 5 winters of spread. (B and C) The maximum (B) and median (C) distance from Schoharie County, maximum distance from the origin will not be complete until the winter of 2037–2038. (D) The convex hull of infection area is the total area within the minimum convex polygon of infected county centroids.



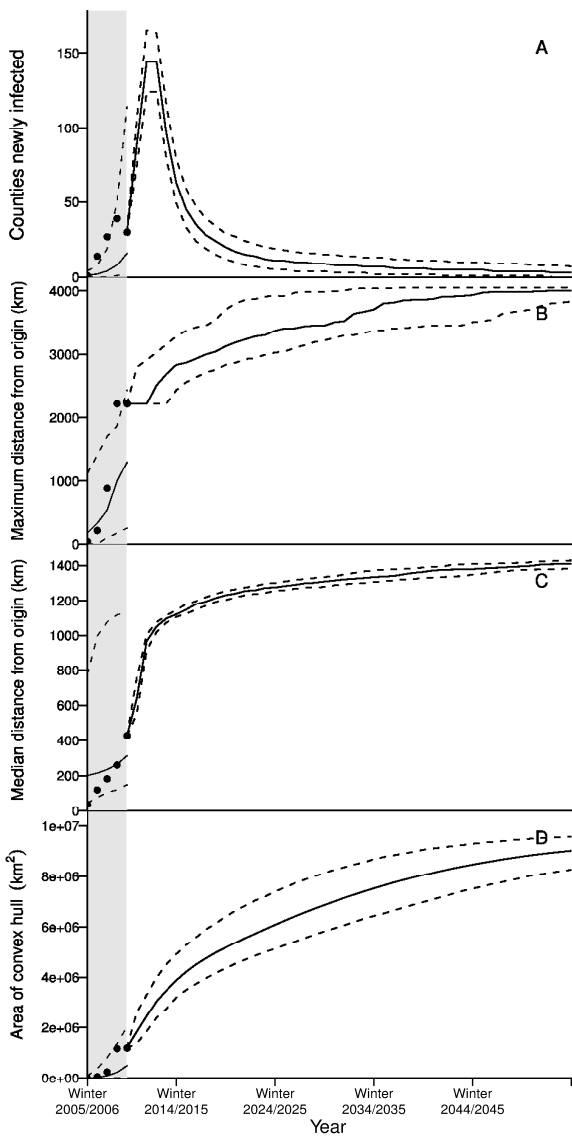
Supplementary Figure S9. Spread statistics for WNS based on the simple diffusion model constrained to counties with caves ML parameter set. Grey shading represents simulated spread from the Schoharie County, NY, and unshaded represents the results simulating from current (2010–2011) observations. Solid lines are median values and dotted lines represent 95% predictive interval. (A) The number of newly infected counties in the given winter, spread peaks in the winter of 2013–2014, although infection rate is not consistent with observations in the first 5 winters of spread. (B and C) The maximum (B) and median (C) distance from Schoharie County, maximum distance from the origin will not be complete until the winter of 2038–2039. (D) The convex hull of infection area is the total area within the minimum convex polygon of infected county centroids.



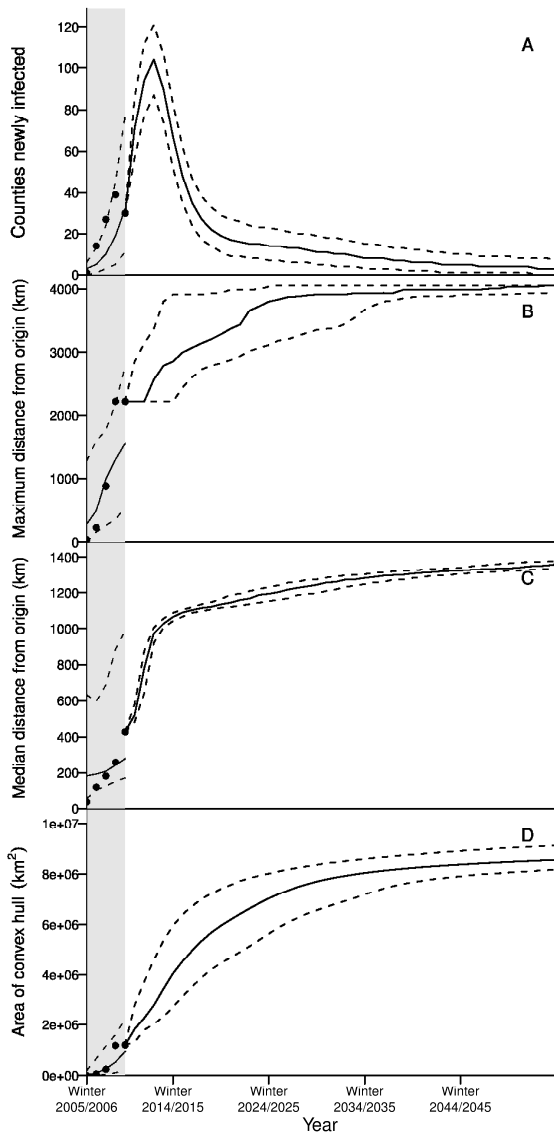
Supplementary Figure S10. Spread statistics for WNS based on the simple diffusion with long-distance dispersal model for the contiguous United States ML parameter set. Grey shading represents simulated spread from the Schoharie County, NY, and unshaded represents the results simulating from current (2010–2011) observations. Solid lines are median values and dotted lines represent 95% predictive interval. (A) The number of newly infected counties in the given winter, spread peaks in the winter of 2015–2016, although infection rate is not consistent with observations in the first 5 winters of spread. (B and C) The maximum (B) and median (C) distance from Schoharie County, maximum distance from the origin will not be complete until the winter of 2034–2035. (D) The convex hull of infection area is the total area within the minimum convex polygon of infected county centroids.



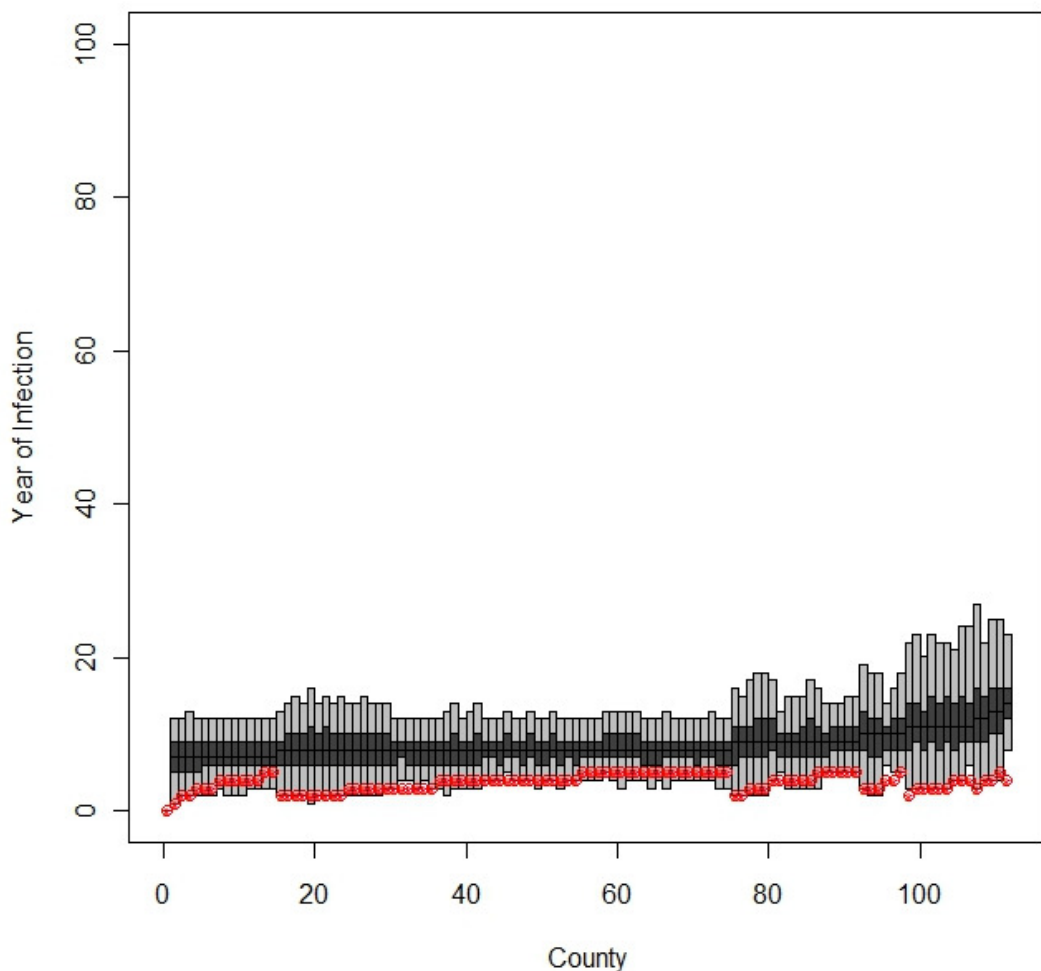
Supplementary Figure S11. Spread statistics for WNS based on the simple diffusion with long-distance dispersal model constrained to counties with caves ML parameter set. Grey shading represents simulated spread from the Schoharie County, NY, and unshaded represents the results simulating from current (2010–2011) observations. Solid lines are median values and dotted lines represent 95% predictive interval. (A) The number of newly infected counties in the given winter, spread peaks in the winter of 2013–2014, although infection rate is not consistent with observations in the first 5 winters of spread. (B and C) The maximum (B) and median (C) distance from Schoharie County, maximum distance from the origin will not be complete until the winter of 2032–2033. (D) The convex hull of infection area is the total area within the minimum convex polygon of infected county centroids.



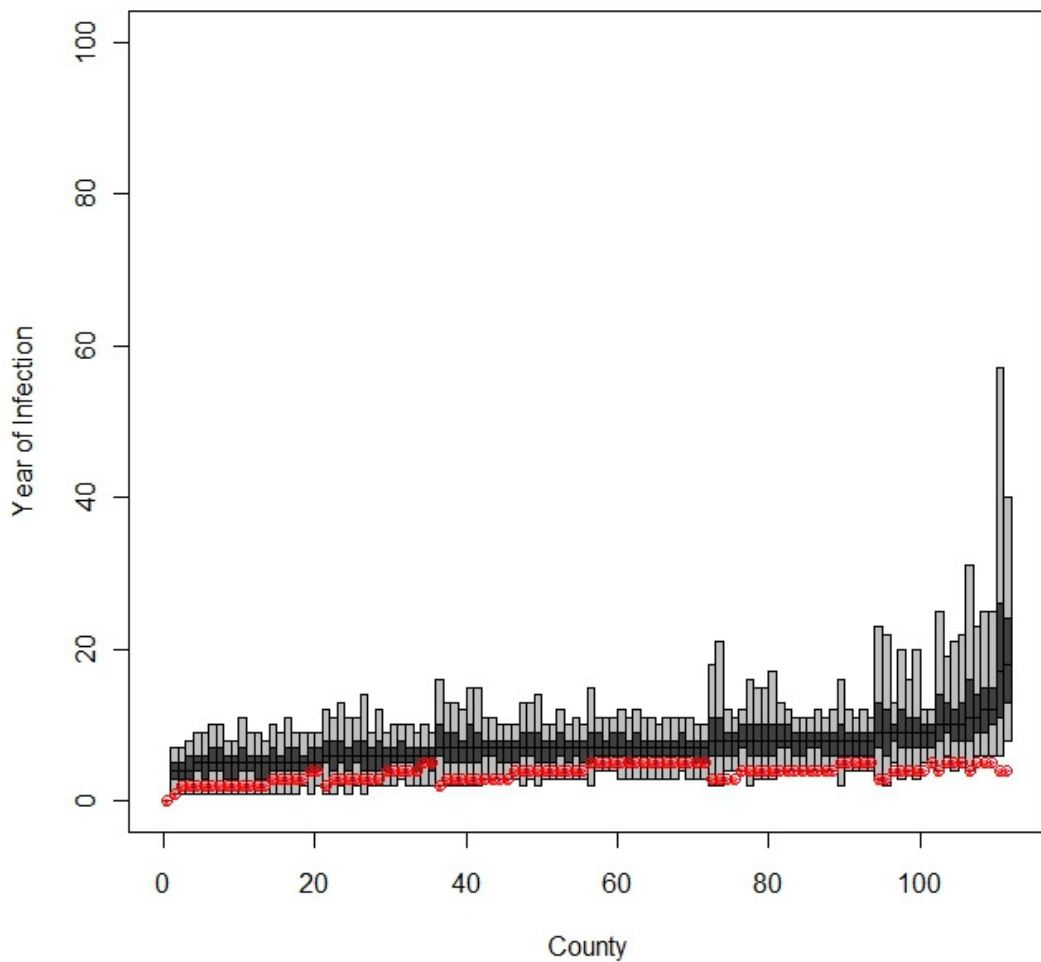
Supplementary Figure S12 Spread statistics for WNS based on the gravity_{caves} model ML parameter set. Grey shading represents simulated spread from the Schoharie County, NY, and unshaded represents the results simulating from current (2010–2011) observations. Solid lines are median values and dotted lines represent 95% predictive interval. (A) The number of newly infected counties in the given winter, spread peaks in the winter of 2013–2014, although infection rate is not consistent with observations in the first 5 winters of spread. (B and C) The maximum (B) and median (C) distance from Schoharie County, maximum distance from the origin will not be complete until the winter of 2065–2066. (D) The convex hull of infection area is the total area within the minimum convex polygon of infected county centroids.



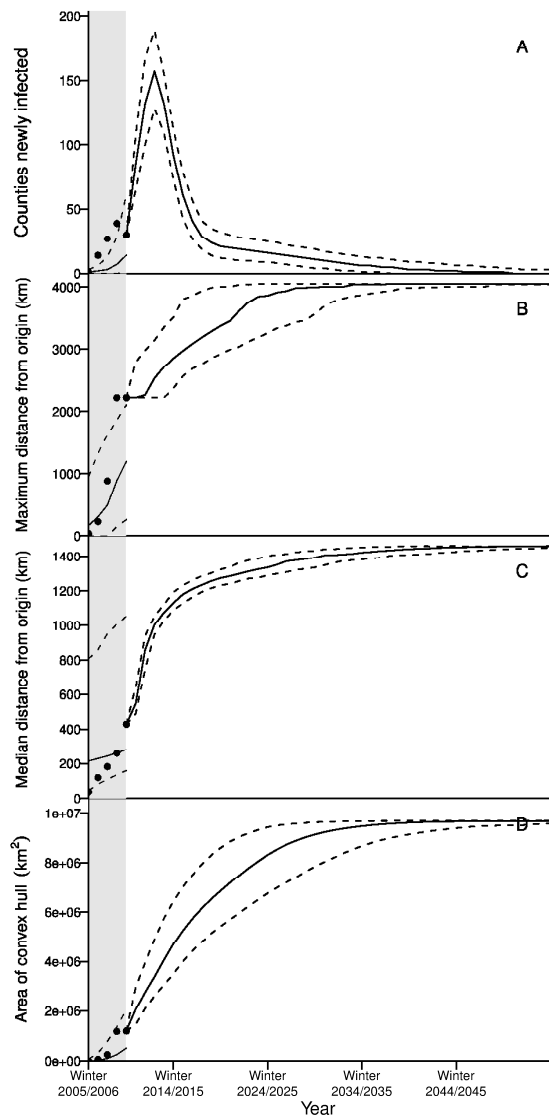
Supplementary Figure S13. Spread statistics for WNS based on the $\text{gravity}_{\text{caves}} + \text{northing}$ model ML parameter set. Grey shading represents simulated spread from the Schoharie County, NY, and unshaded represents the results simulating from current (2010–2011) observations. Solid lines are median values and dotted lines represent 95% predictive interval. (A) The number of newly infected counties in the given winter, spread peaks in the winter of 2013–2014, and infection rate is reasonably consistent with observations in the first 5 winters of spread. (B and C) The maximum (B) and median (C) distance from Schoharie County, maximum distance from the origin will not be complete until the winter of 2054–2055. (D) The convex hull of infection area is the total area within the minimum convex polygon of infected county centroids.



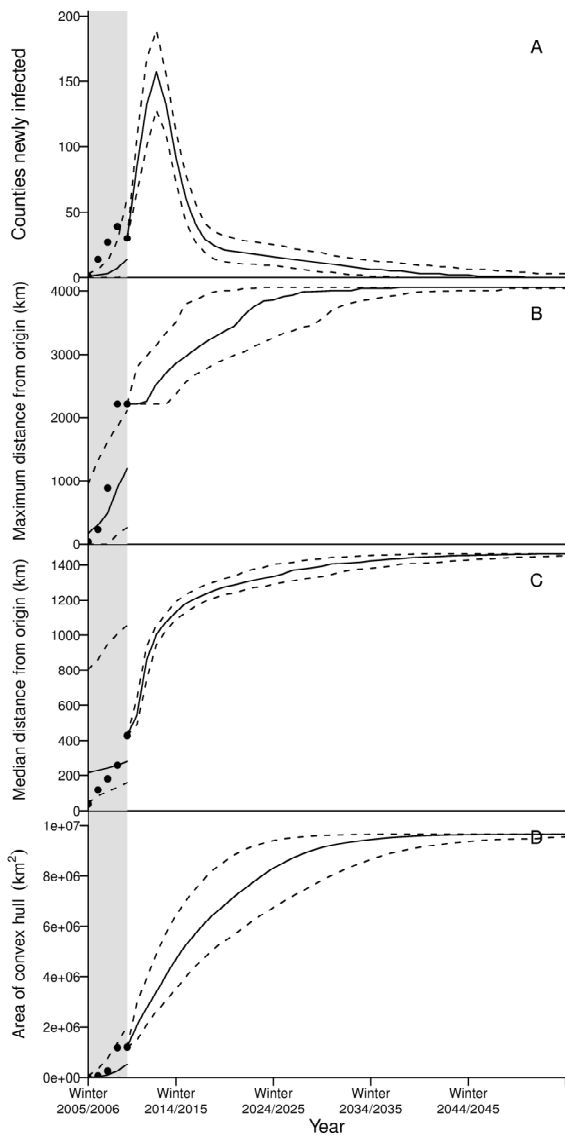
Supplementary Figure S14. The predicted year of infection for the currently (2010–2011) observed infected counties based on simulations from Schoharie County using the $\text{gravity}_{\text{caves}}$ model ML parameter set. For each county, the 95% prediction interval is in grey with the interquartile range specified by dark grey, with the simulated mean infection year as a black bar; red dots represent the observed year of infection for that county. Counties are ordered by the simulated year of infection. Observations are usually within the predictive interval (102 of 112 counties).



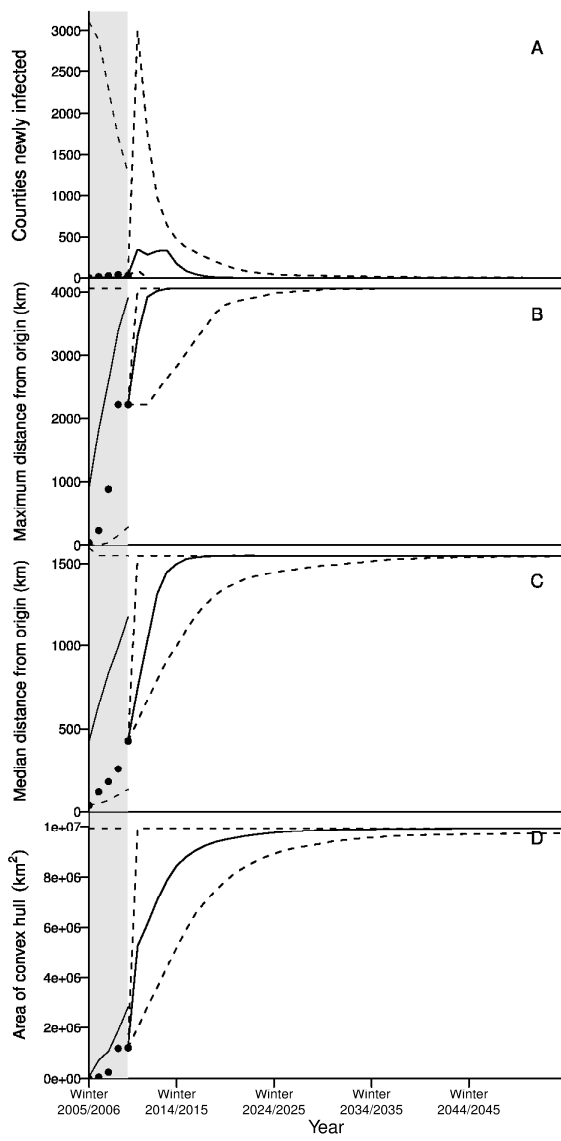
Supplementary Figure S15. The predicted year of infection for the currently (2010–2011) observed infected counties based on simulations from Schoharie County using the gravity_{caves+northing} model ML parameter set. For each county, the 95% prediction interval is in grey with the interquartile range specified by dark grey, with the simulated mean infection year as a black bar; red dots represent the observed year of infection for that county. Counties are ordered by the simulated year of infection. Observations are usually within the predictive interval (102 of 112 counties).



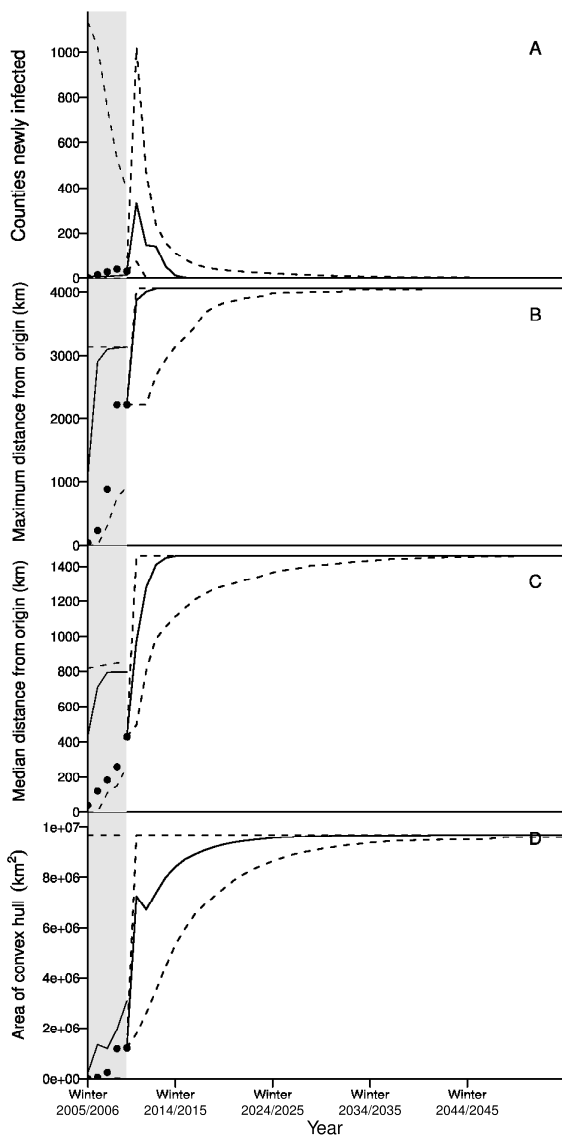
Supplementary Figure S16. Spread statistics for WNS based on the simple diffusion model for the contiguous United States SU parameter set. Grey shading represents simulated spread from the Schoharie County, NY, and unshaded represents the results simulating from current (2010–2011) observations. Solid lines are median values and dotted lines represent 95% predictive interval. (A) The number of newly infected counties in the given winter, spread peaks in the winter of 2017–2018, although infection rate is not consistent with observations in the first 5 winters of spread. (B and C) The maximum (B) and median (C) distance from Schoharie County, maximum distance from the origin will not be complete until the winter of 2052–2053. (D) The convex hull of infection area is the total area within the minimum convex polygon of infected county centroids.



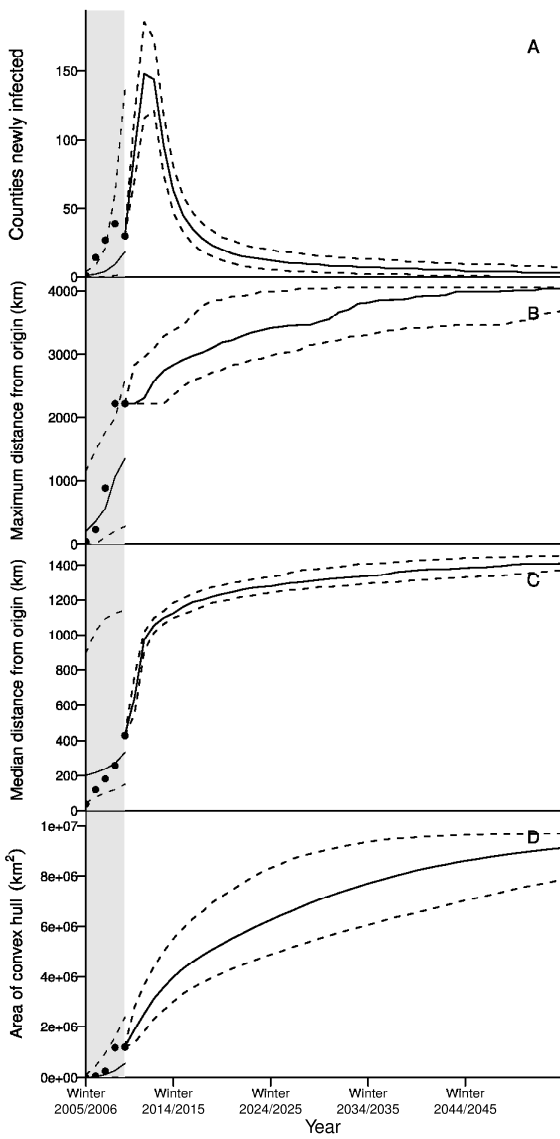
Supplementary Figure. S17. Spread statistics for WNS based on the simple diffusion dispersal model constrained to counties with caves SU parameter set. Grey shading represents simulated spread from the Schoharie County, NY, and unshaded represents the results simulating from current (2010–2011) observations. Solid lines are median values and dotted lines represent 95% predictive interval. (A) The number of newly infected counties in the given winter, spread peaks in the winter of 2013–2014, although infection rate is not consistent with observations in the first 5 winters of spread. (B and C) The maximum (B) and median (C) distance from Schoharie County, maximum distance from the origin will not be complete until the winter of 2038–2039. (D) The convex hull of infection area is the total area within the minimum convex polygon of infected county centroids.



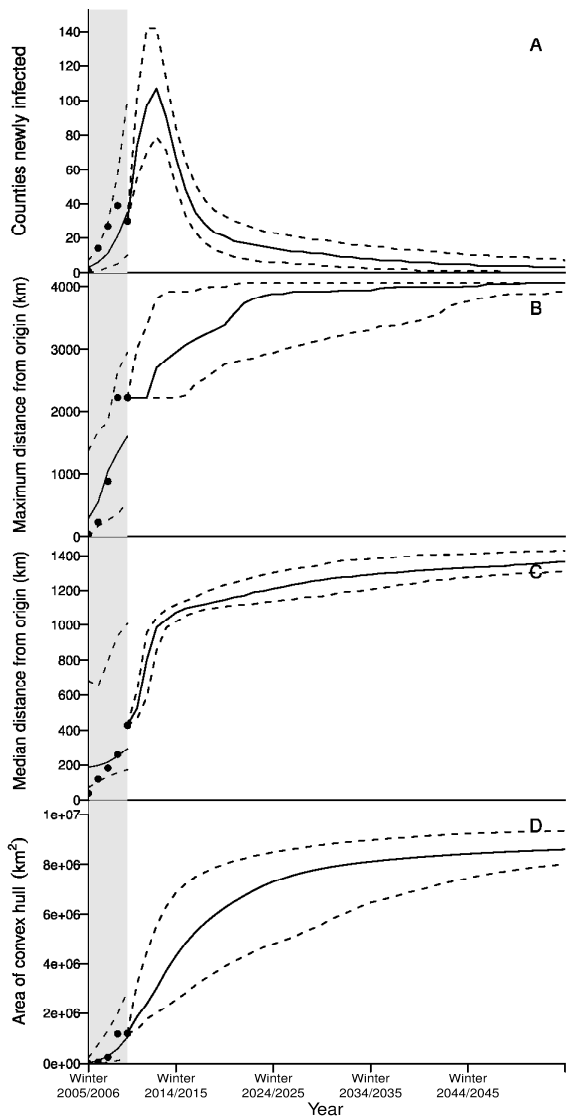
Supplementary Figure S18. Spread statistics for WNS based on the simple diffusion with long-distance dispersal model for the contiguous United States SU parameter set. Grey shading represents simulated spread from the Schoharie County, NY, and unshaded represents the results simulating from current (2010–2011) observations. Solid lines are median values and dotted lines represent 95% predictive interval. (A) The number of newly infected counties in the given winter, spread peaks in the winter of 2014–2015, although uncertainty is quite high for observations in the first 5 winters of spread. (B and C) The maximum (B) and median (C) distance from Schoharie County, maximum distance from the origin will not be complete until the winter of 2016–2017. (D) The convex hull of infection area is the total area within the minimum convex polygon of infected county centroids.



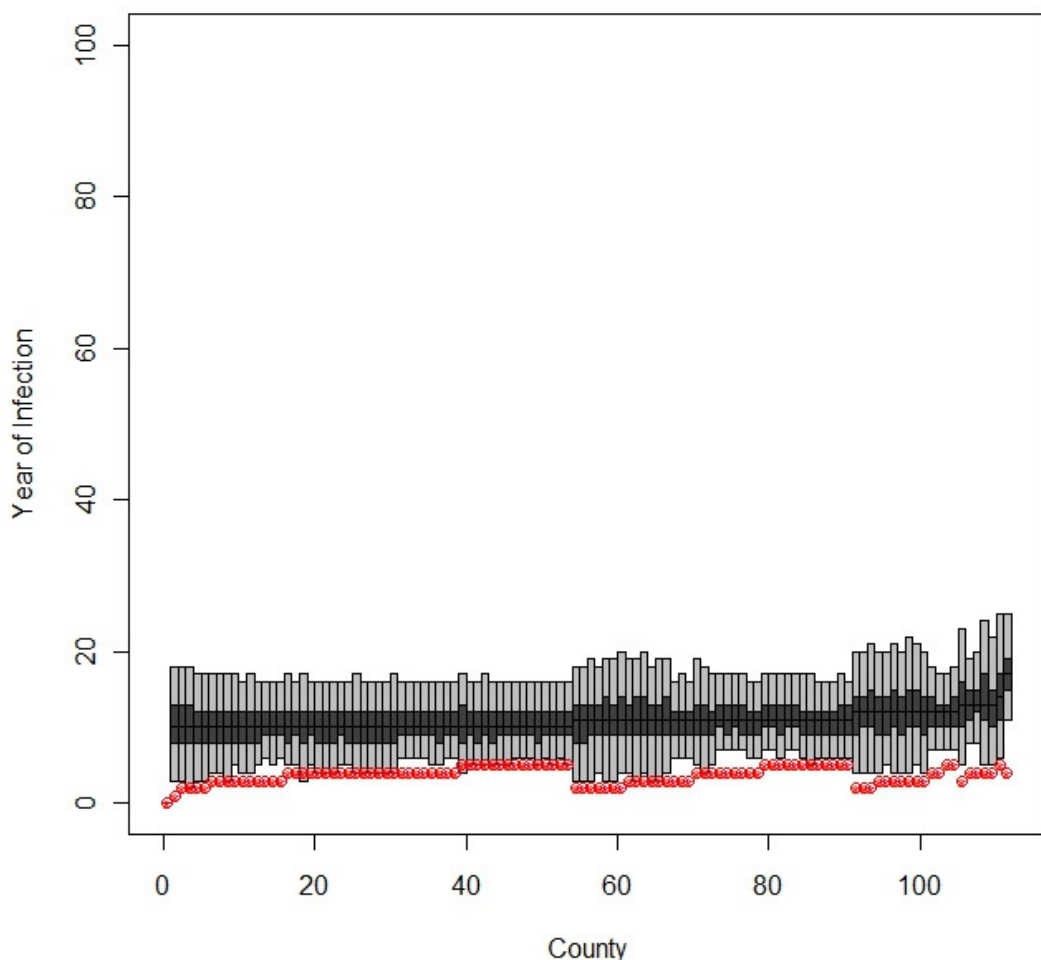
Supplementary Figure S19. Spread statistics for WNS based on the simple diffusion model with long-distance dispersal constrained to counties with caves SU parameter set. Grey shading represents simulated spread from the Schoharie County, NY, and unshaded represents the results simulating from current (2010–2011) observations. Solid lines are median values and dotted lines represent 95% predictive interval. (A) The number of newly infected counties in the given winter, spread peaks in the winter of 2011–2012, although uncertainty is quite high for observations in the first 5 winters of spread. (B and C) The maximum (B) and median (C) distance from Schoharie County, maximum distance from the origin will not be complete until the winter of 2013–2014. (D) The convex hull of infection area is the total area within the minimum convex polygon of infected county centroids.



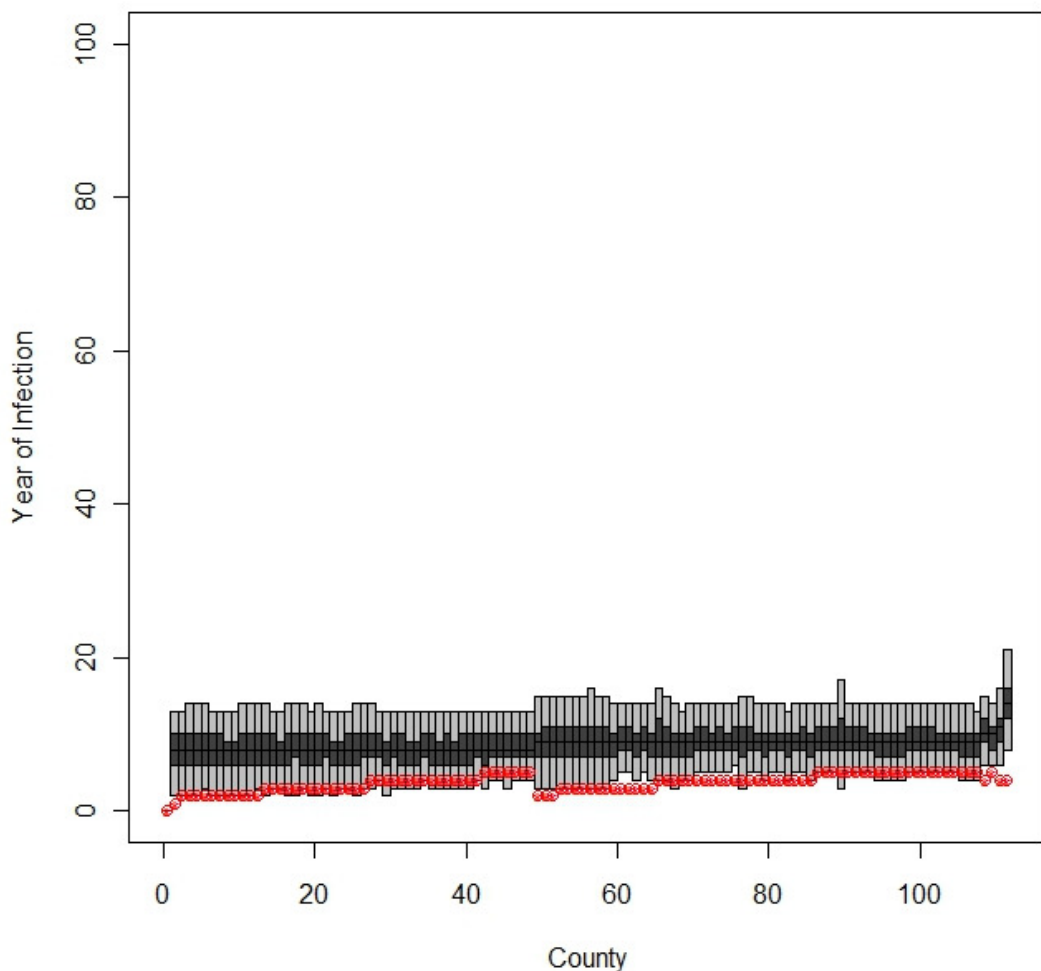
Supplementary Figure S20. Spread statistics for WNS based on the gravity_{caves} model SU parameter set. Grey shading represents simulated spread from the Schoharie County, NY, and unshaded represents the results simulating from current (2010–2011) observations. Solid lines are median values and dotted lines represent 95% predictive interval. (A) The number of newly infected counties in the given winter, spread peaks in the winter of 2012–2013, although infection rate is not consistent with observations in the first 5 winters of spread. (B and C) The maximum (B) and median (C) distance from Schoharie County, maximum distance from the origin will not be complete until the winter of 2062–2063. (D) The convex hull of infection area is the total area within the minimum convex polygon of infected county centroids.



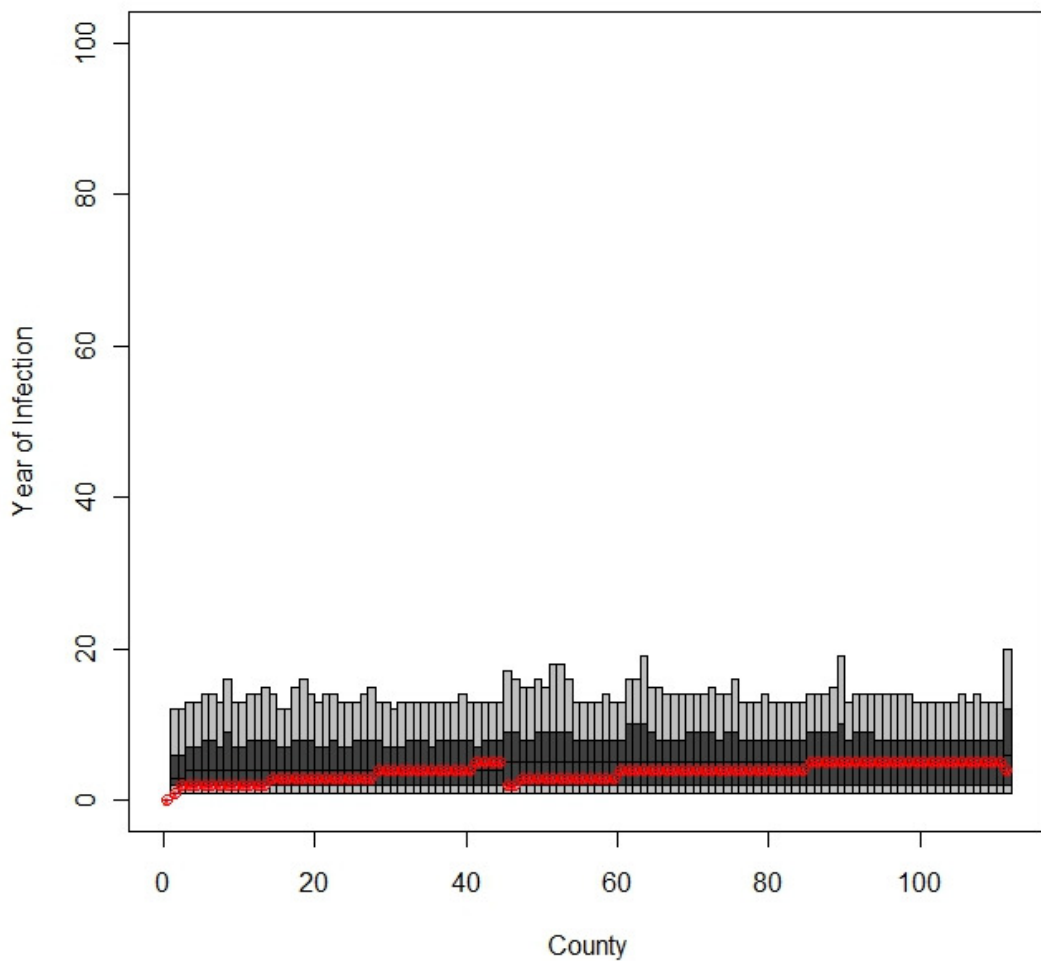
Supplementary Figure S21. Spread statistics for WNS based on the gravity_{caves+northing} model SU parameter set. Grey shading represents simulated spread from the Schoharie County, NY, and unshaded represents the results simulating from current (2010–2011) observations. Solid lines are median values and dotted lines represent 95% predictive interval. (A) The number of newly infected counties in the given winter, spread peaks in the winter of 2013–2014, although infection rate is not consistent with observations in the first 5 winters of spread. (B and C) The maximum (B) and median (C) distance from Schoharie County, maximum distance from the origin will not be complete until the winter of 2051–2052. (D) The convex hull of infection area is the total area within the minimum convex polygon of infected county centroids.



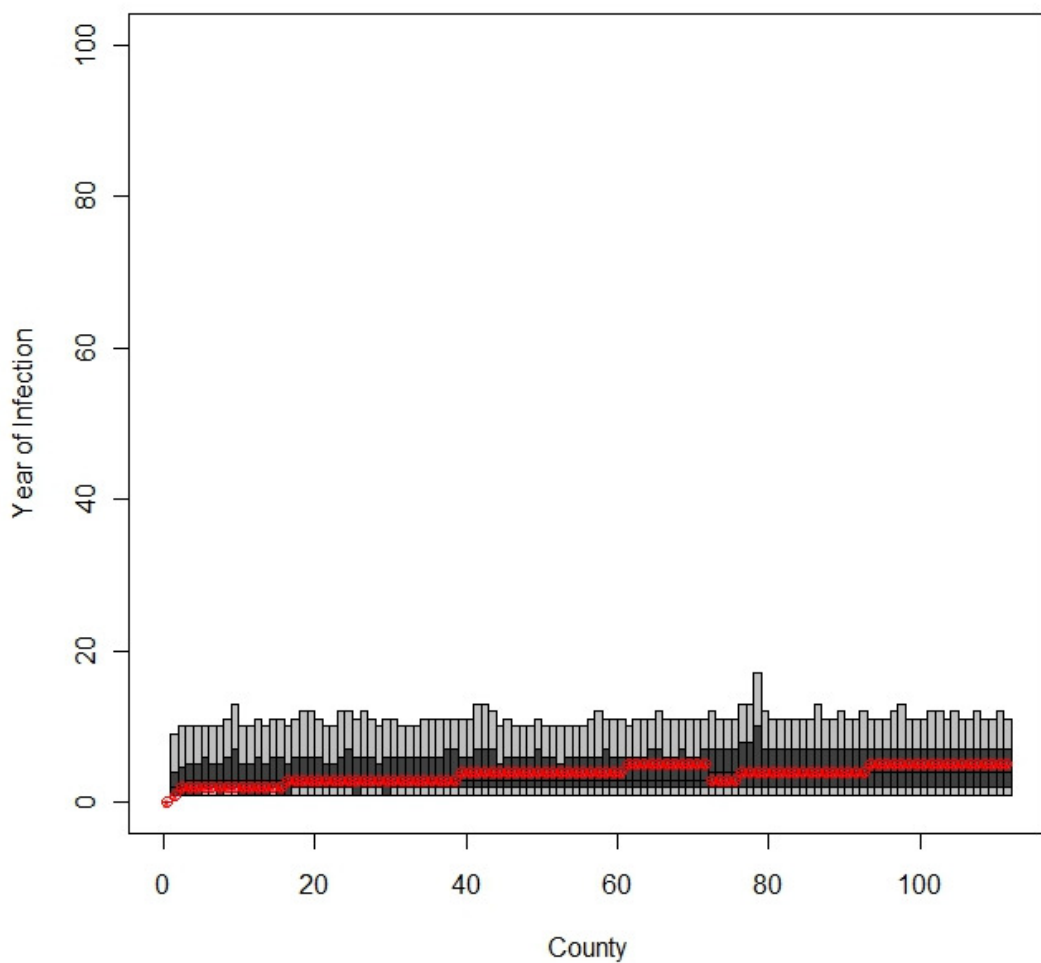
Supplementary Figure S22. The predicted year of infection for the currently (2010–2011) observed infected counties based on simulations from Schoharie County using the simple diffusion model constrained to counties with caves under the SU parameter set. For each county, the 95% confidence range is in grey with the interquartile range specified by dark grey, with the simulated mean infection year as a black bar; red dots represent the observed year of infection for that county. Counties are ordered by the simulated year of infection. The model was able to estimate the given year of infection for a small subset of counties (28 of 112 counties).



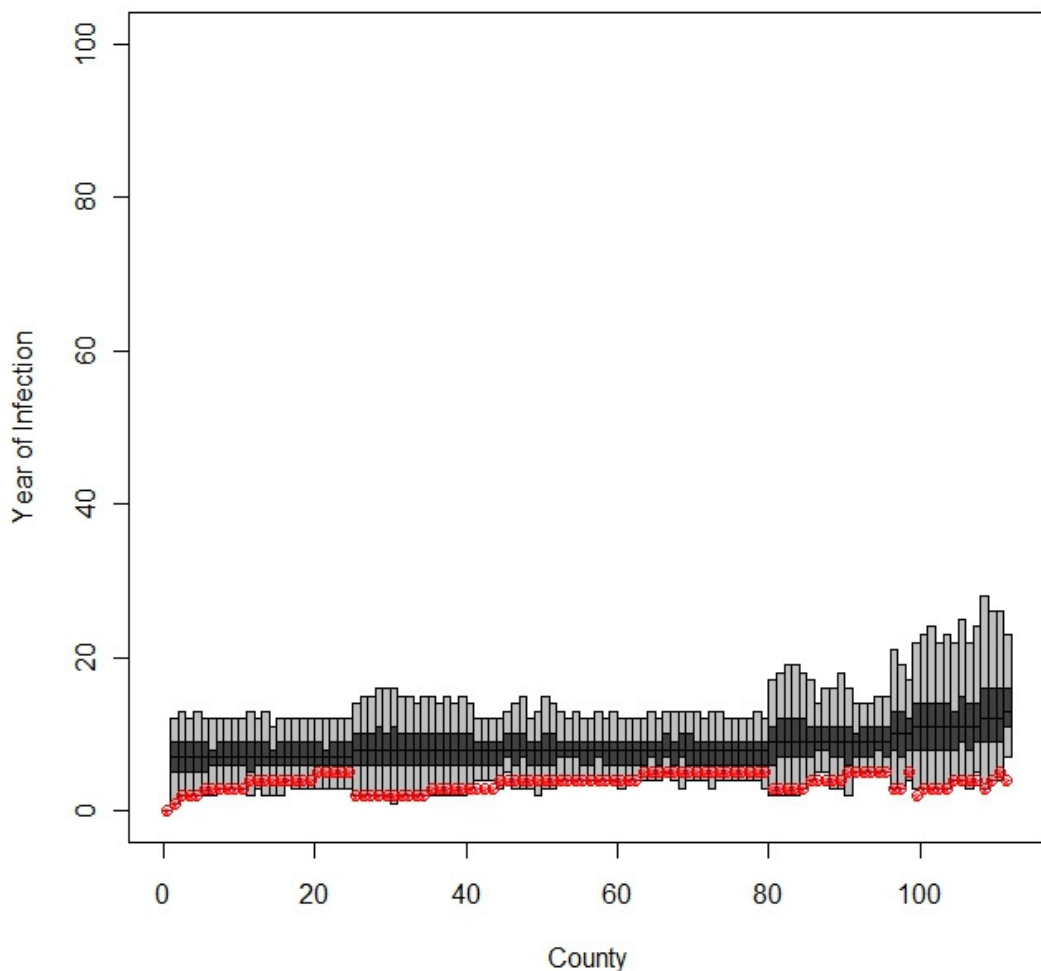
Supplementary Figure S23. The predicted year of infection for the currently (2010–2011) observed infected counties based on simulations from Schoharie County using the simple diffusion model constrained to counties with caves under the SU parameter set. For each county, the 95% confidence range is in grey with the interquartile range specified by dark grey, with the simulated mean infection year as a black bar; red dots represent the observed year of infection for that county. Counties are ordered by the simulated year of infection. The model was able to estimate the given year of infection for the majority of counties (84 of 112 counties).



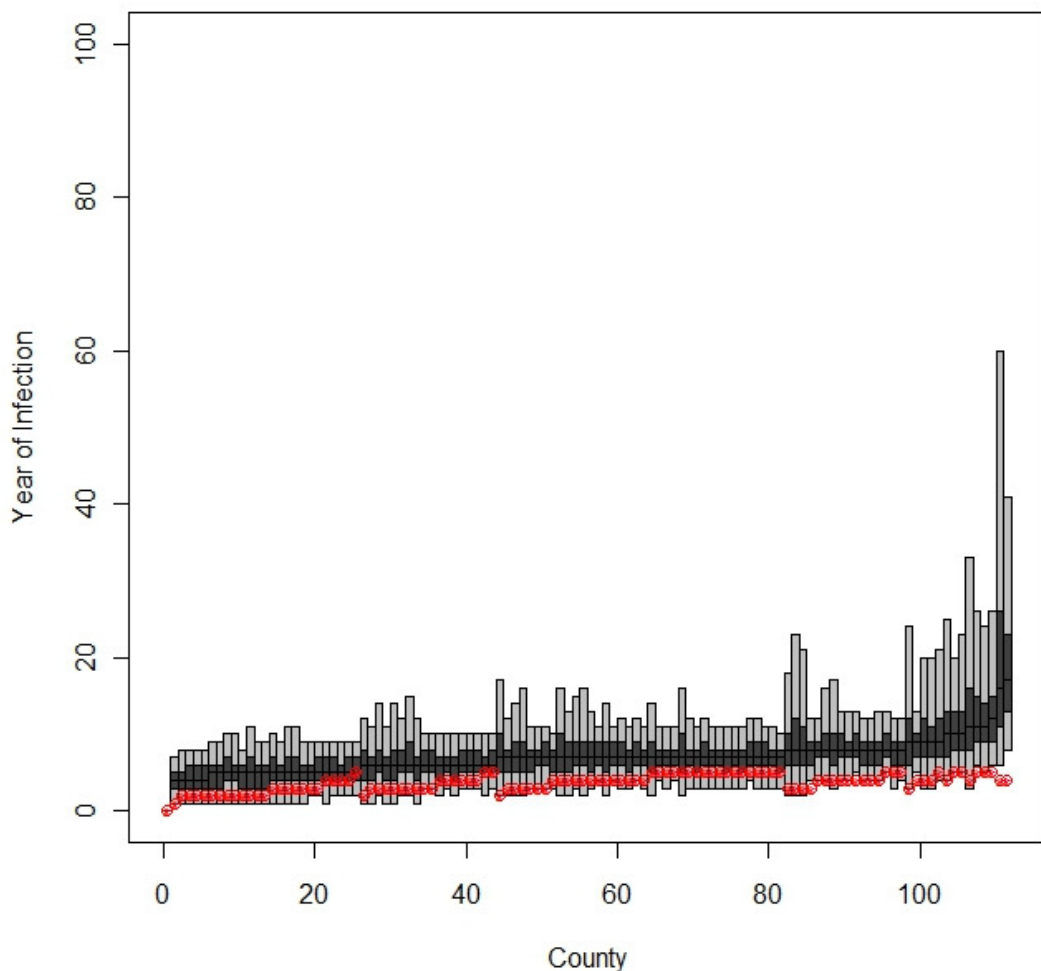
Supplementary Figure S24. The predicted year of infection for the currently (2010–2011) observed infected counties based on simulations from Schoharie County using the simple diffusion with long-distance dispersal model for the contiguous United States under the SU parameter set. For each county, the 95% confidence range is in grey with the interquartile range specified by dark grey, with the simulated mean infection year as a black bar; red dots represent the observed year of infection for that county. Counties are ordered by the simulated year of infection. The model was able to estimate the given year of infection for all counties, although many over-estimated.



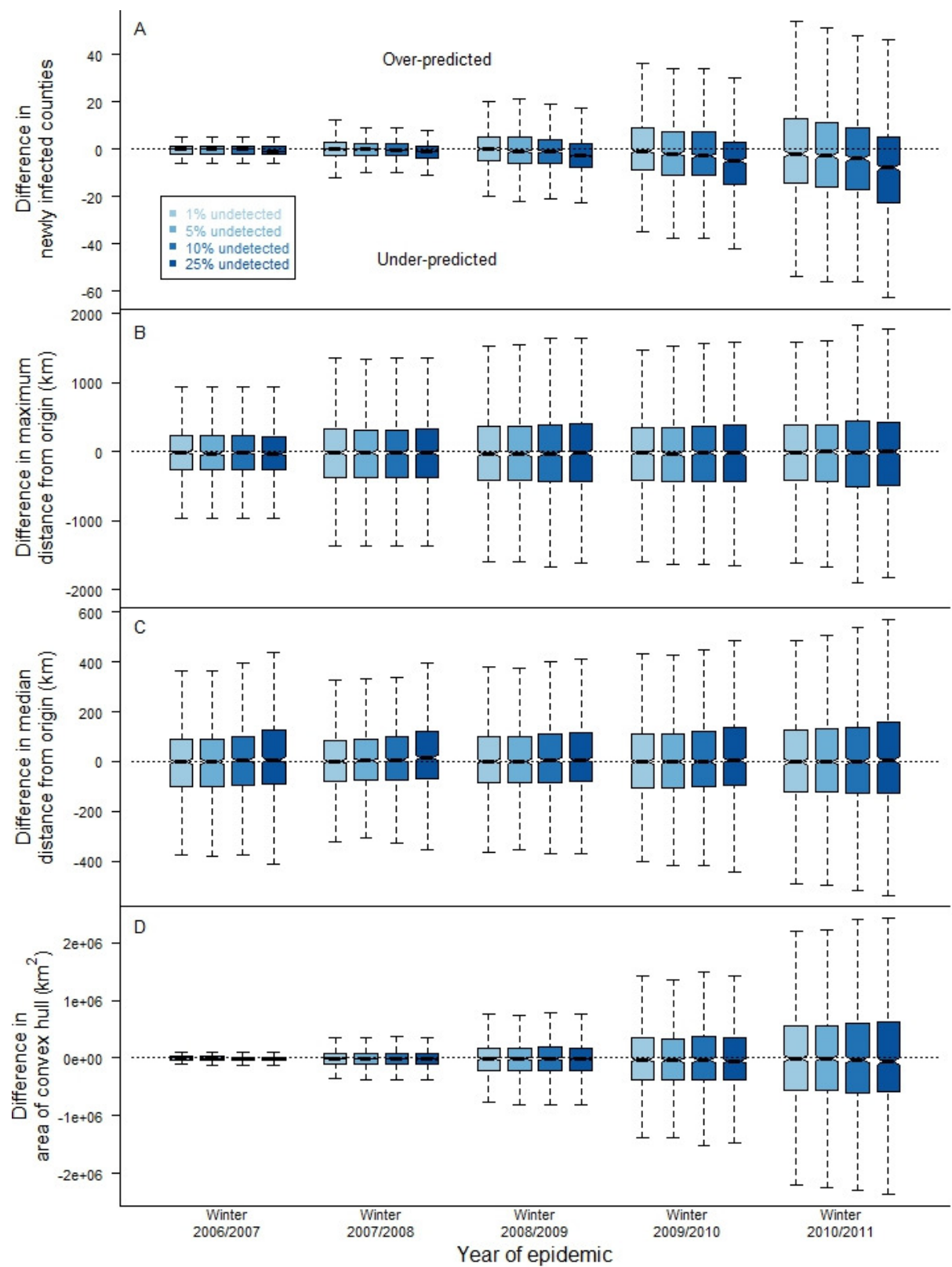
Supplementary Figure S25. The predicted year of infection for the currently (2010–2011) observed infected counties based on simulations from Schoharie County using the simple diffusion model constrained to counties with caves under the SU parameter set. For each county, the 95% confidence range is in grey with the interquartile range specified by dark grey, with the simulated mean infection year as a black bar; red dots represent the observed year of infection for that county. Counties are ordered by the simulated year of infection. The model was able to estimate the given year of infection for all counties, although many were overestimated.



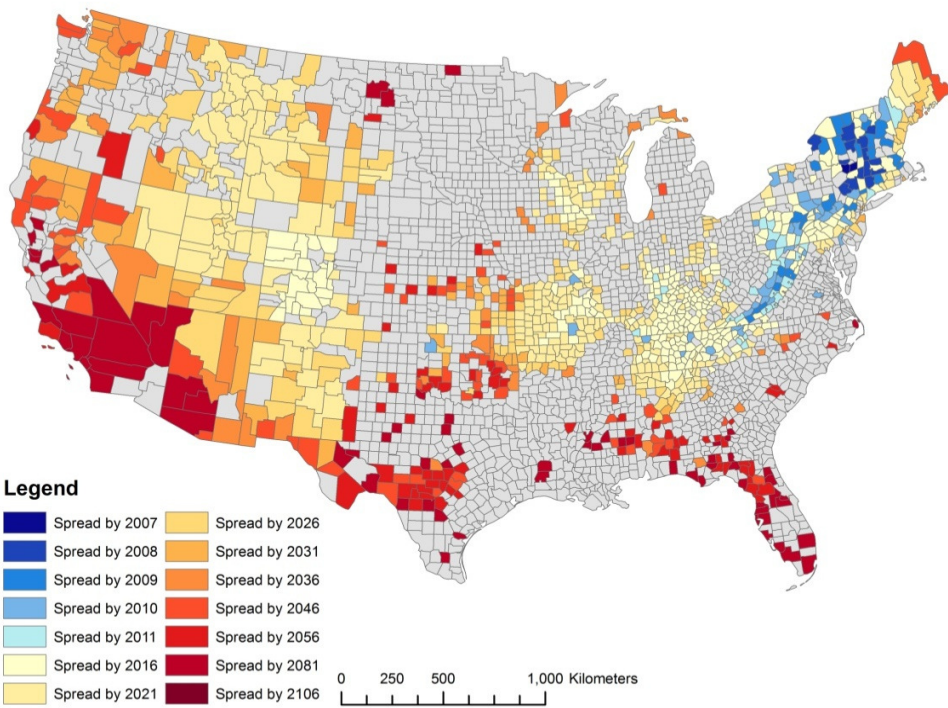
Supplementary Figure S26. The predicted year of infection for the currently (2010–2011) observed infected counties based on simulations from Schoharie County using the $\text{gravity}_{\text{caves}}$ model under the SU parameter set. For each county, the 95% confidence range is in grey with the interquartile range specified by dark grey, with the simulated mean infection year as a black bar; red dots represent the observed year of infection for that county. Counties are ordered by the simulated year of infection. The model was able to estimate the given year of infection for most of the counties (105 of 112 counties).



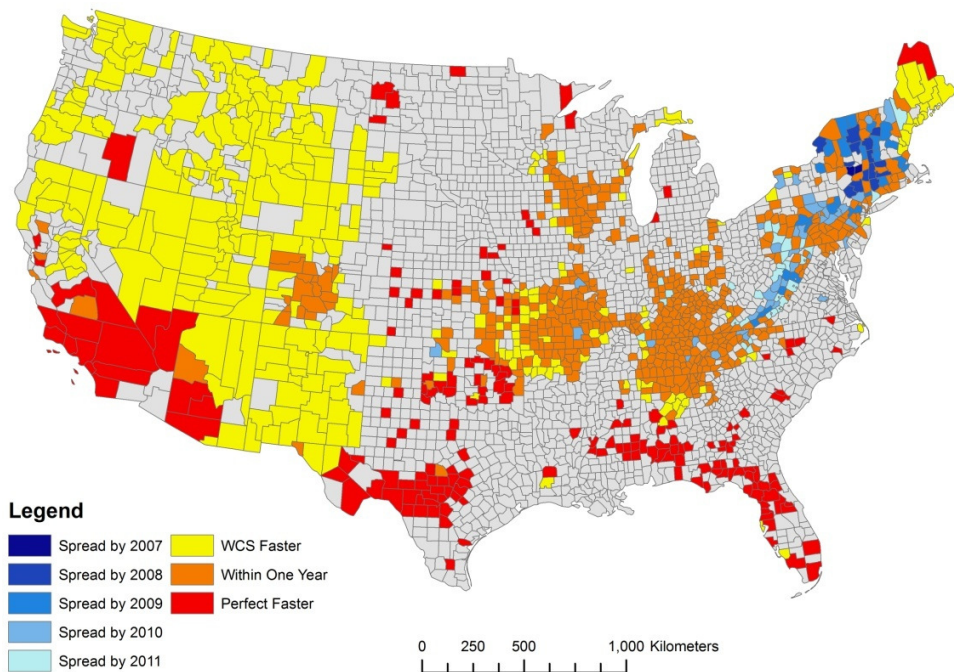
Supplementary Figure S27. The predicted year of infection for the currently (2010–2011) observed infected counties based on simulations from Schoharie County using the $\text{gravity}_{\text{caves+northing}}$ model under the SU parameter set. For each county, the 95% confidence range is in grey with the interquartile range specified by dark grey, with the simulated mean infection year as a black bar; red dots represent the observed year of infection for that county. Counties are ordered by the simulated year of infection. The model was able to estimate the given year of infection for most of the counties (105 of 112 counties).



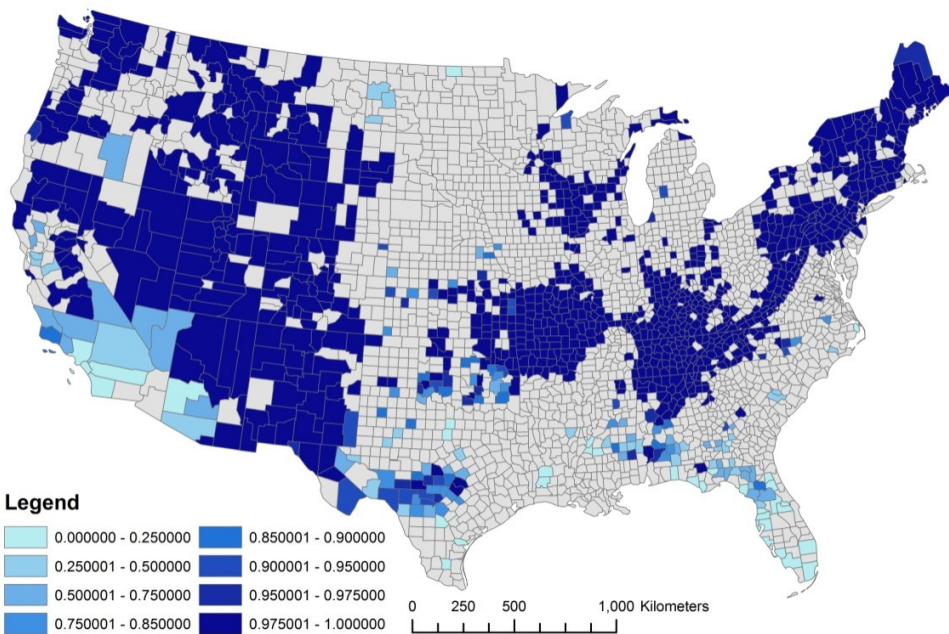
Supplementary Figure S28 (Previous page). Box-whisker plot of bias in summary statistics caused by imperfect detection of WNS infection. Bias was calculated as: (statistic in imperfect detection simulations – statistic in the fully detected simulations), negative values represent under-estimates. Imperfect detection simulations used maximum likelihood estimates of β s for the gravity_{caves+winter} model fitted to 1000 infection histories where 1%, 5%, 10%, and 25% (shades of blue) of infected counties were randomly undetected (see Methods for more detail). The β estimates were then used to simulate from the origin for 5 years, representing a new estimate of the epidemic spread. A) Difference in number of newly infected counties in each of first 5 years; B) maximum distance spread at end of each of first 5 years (km); C) median distance spread at end of each of first 5 years; and D) area of convex hull for infected counties at end of each of first 5 years. Boxes are interquartile range on each side of the media, with whiskers extending to 1.5 times the length of the box away from the box. Notches are $\pm 1.58 \times$ interquartile range/ $\sqrt{\text{sample size}}$, indicating the approximate 95% CI for the difference in medians. Overlap of notches with dotted line at $y=0$ represents no difference between imperfect detection and full detection.



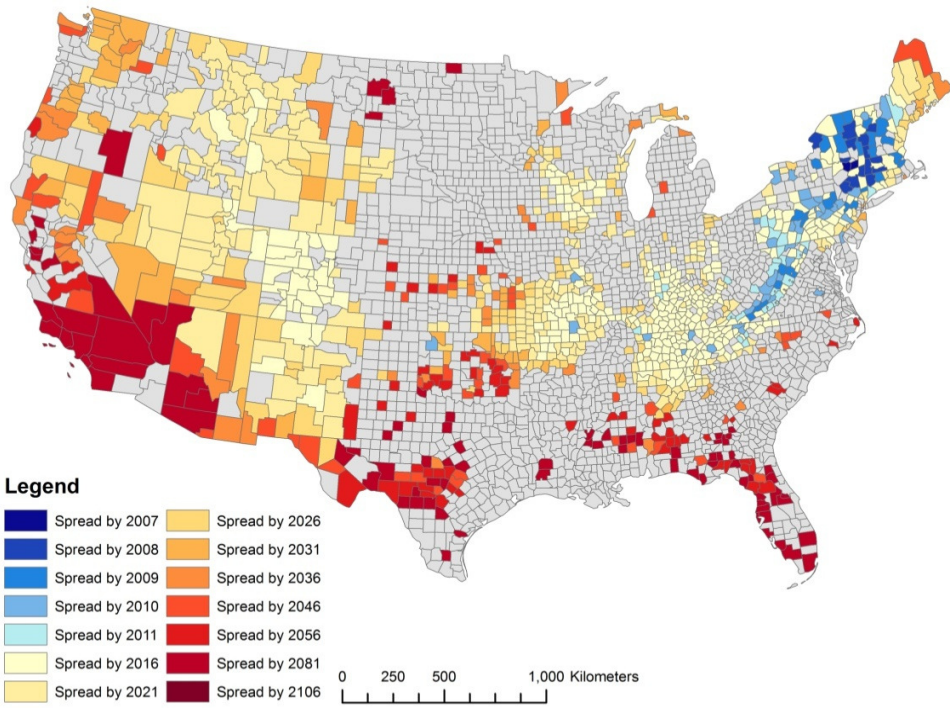
Supplementary Figure S29. Observed year of infection and mean estimated year of infection under the gravity_{caves} + winter model using the maximum likelihood parameters for the 25% underdetection scenario and observed climate data. Estimated infection (yellow-to-red scale) is predicted from simulations begun from currently infected counties (2010-2011; blue color scale). Grey counties did not have reported caves or WNS observations. There is a strong qualitative similarity to results when assuming perfect detection.



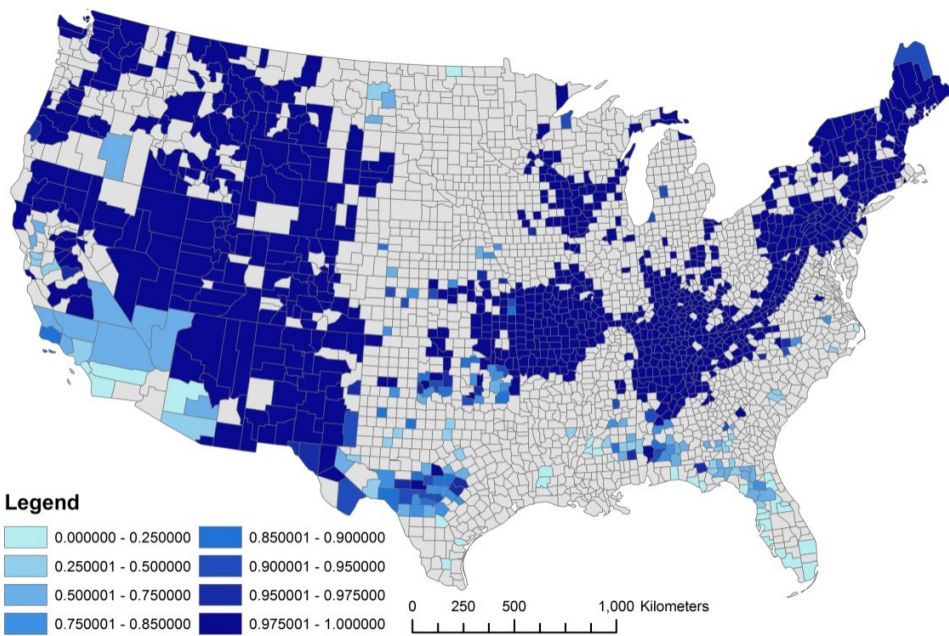
Supplementary Figure S30. Difference in the mean predicted year of infection for the 25% underdetection (Worst Case Scenario, WCS) and assumed perfect detection using the observed climate data. Yellow represents counties ($n=304$) where the WCS was faster (mean=1.84 years, maximum=4.78 years); red represents counties ($n=187$) where assumed perfect detection is faster (mean=4.66 years, maximum 11.4 years); orange counties are essentially equivalent between the two scenarios. Currently infected counties are shown in blue color scale.



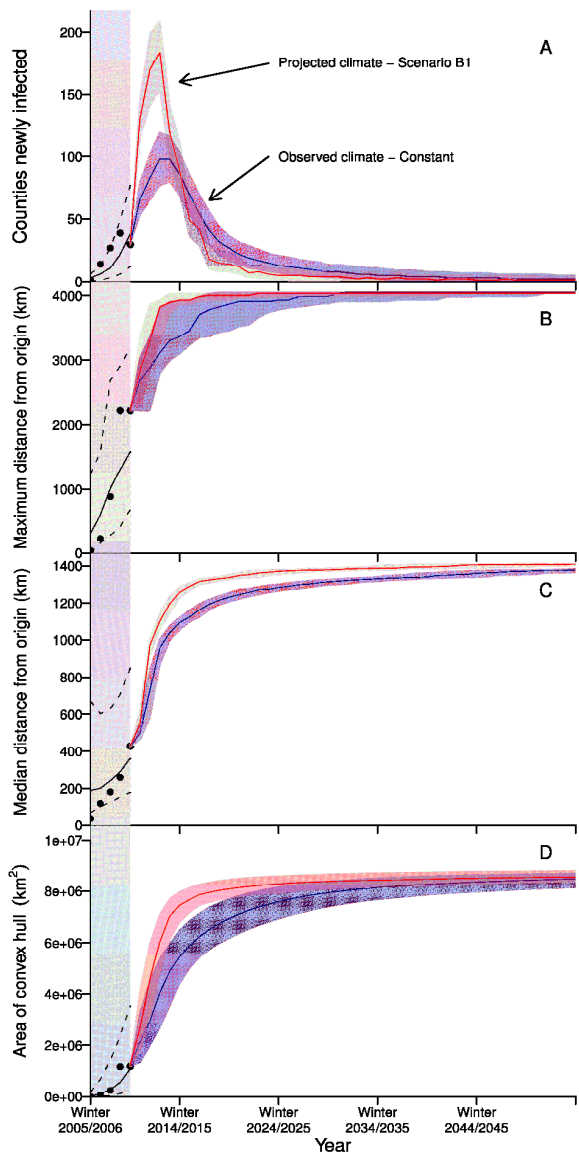
Supplementary Figure S31. The frequency of counties becoming infected by the winter of 2105–2106 under the $\text{gravity}_{\text{caves}} + \text{winter}$ model using the ML parameter set. Counties in southern California and southern Florida were not always reached, but most the remaining counties with caves are likely to be infected.



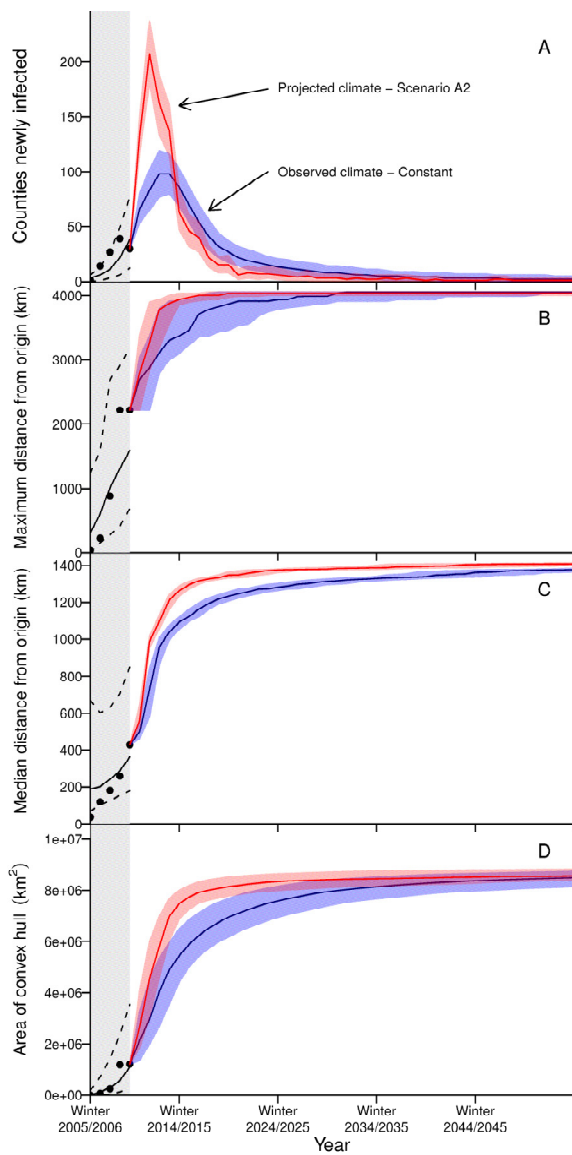
Supplementary Figure S32. Mean estimated year of infection, when infection (yellow-to-red scale) is predicted from simulations begun from currently infected counties (2010–2011; blue color scale) under the gravity_{caves+winter} model using the SU parameter set. Grey counties did not have reported caves or WNS observations. The model predicts spread to most (93% P.I. 90%–97%) of the counties with caves in the contiguous United States within a century of the first infection, many within the next 20 years. Spread to the southeast is slow as is spread to the southwest; longer time to infection in the Upper Midwest and New England may be due to edge effects (see Discussion).



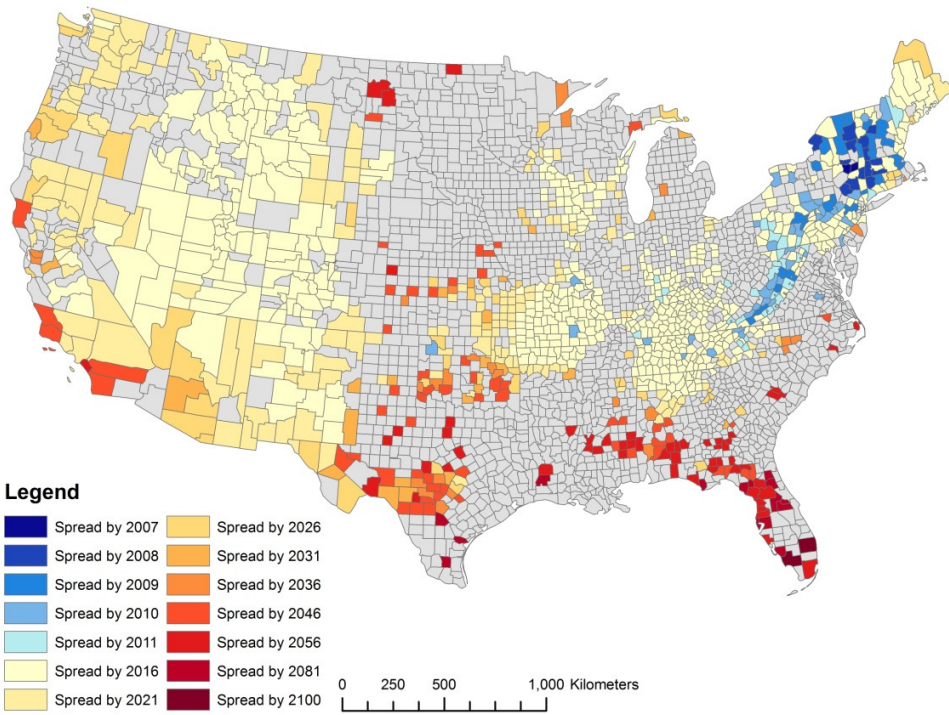
Supplementary Figure S33. The frequency of counties becoming infected by the winter of 2105–2106 under the gravity_{caves}+winter model using the SU parameter set. Counties in southern California and southern Florida were not always reached, but most the remaining counties with caves are likely to be infected.



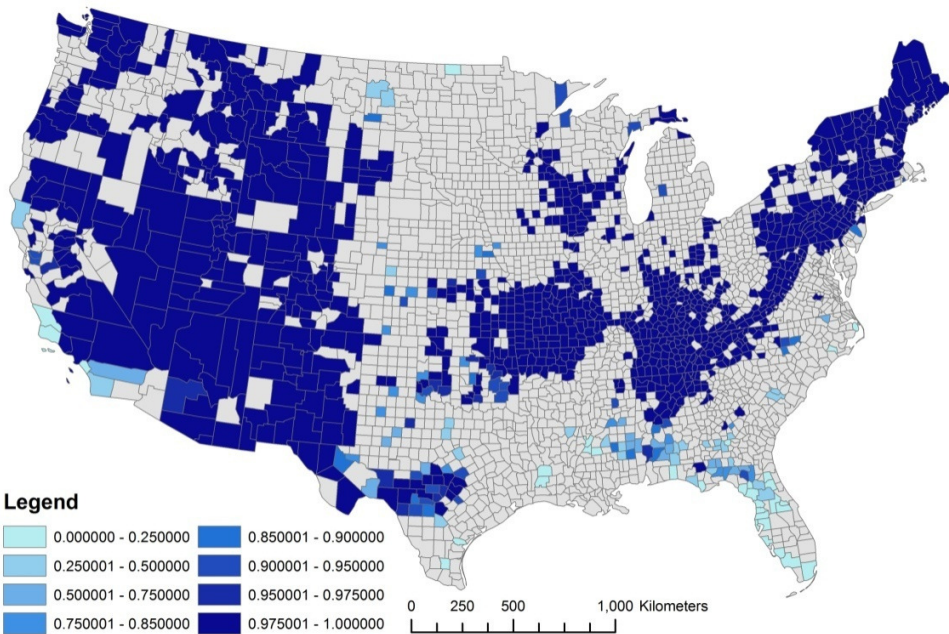
Supplementary Figure S34. Spread statistics for WNS based on the gravity_{caves+winter} model maximum likelihood parameter set including statistics for SRES B1 climate scenario. Grey shading represents simulated spread from Schoharie County, NY, to the present and unshaded represents forecasts obtained by forward simulation from the current (2010-2011) state. Simulations forward were based on climate remaining as observed during the epidemic (blue) or as projected under the SRES B1 climate scenario (red), which tended to have longer winters (see Supplementary Methods). Solid lines are median values and dotted lines/shaded areas represent 95% prediction intervals. (A) The number of newly infected counties in the given winter; spread peaks in the winter of 2013-2014, and infection rate is consistent with observations in the first 5 winters of spread. (B and C) The maximum (B) and median (C) distance from Schoharie County; maximum distance from the origin will not be complete until the winter of 2032-2033. (D) The convex hull of infection area is the total area within the minimum convex polygon of infected county centroids.



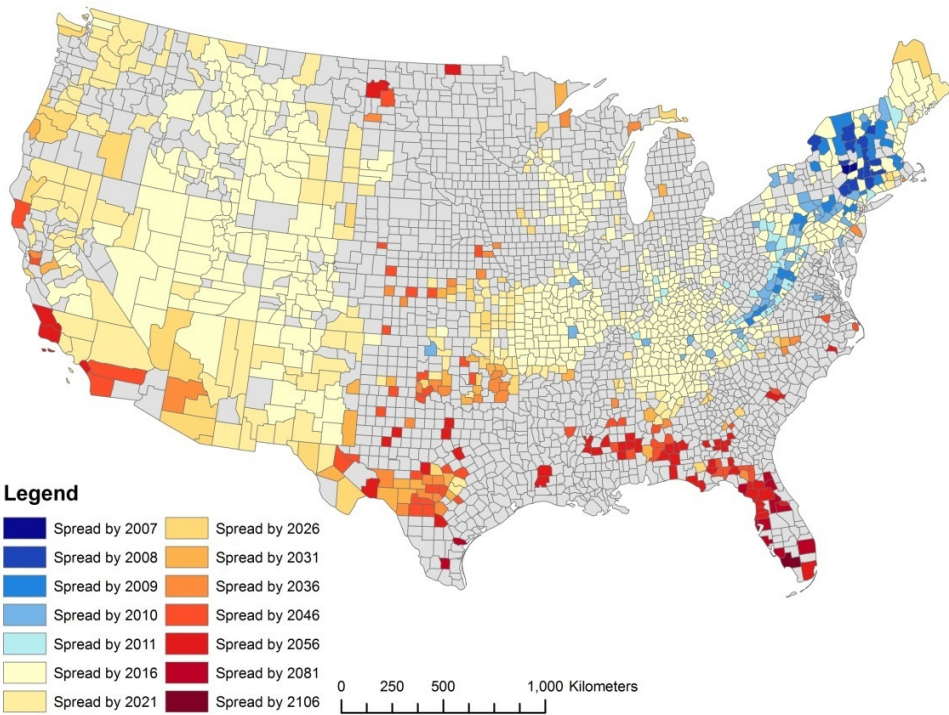
Supplementary Figure S35. Spread statistics for WNS based on the gravity_{caves+winter} model maximum likelihood parameter set including statistics for SRES A2 climate scenario. Grey shading represents simulated spread from Schoharie County, NY, to the present and unshaded represents forecasts obtained by forward simulation from the current (2010-2011) state. Simulations forward were based on climate remaining as observed during the epidemic (blue) or as projected under the SRES A2 climate scenario (red), which tended to have longer winters (see Supplementary Methods). Solid lines are median values and dotted lines/shaded areas represent 95% prediction intervals. (A) The number of newly infected counties in the given winter; spread peaks in the winter of 2013-2014, and infection rate is consistent with observations in the first 5 winters of spread. (B and C) The maximum (B) and median (C) distance from Schoharie County; maximum distance from the origin will not be complete until the winter of 2032-2033. (D) The convex hull of infection area is the total area within the minimum convex polygon of infected county centroids.



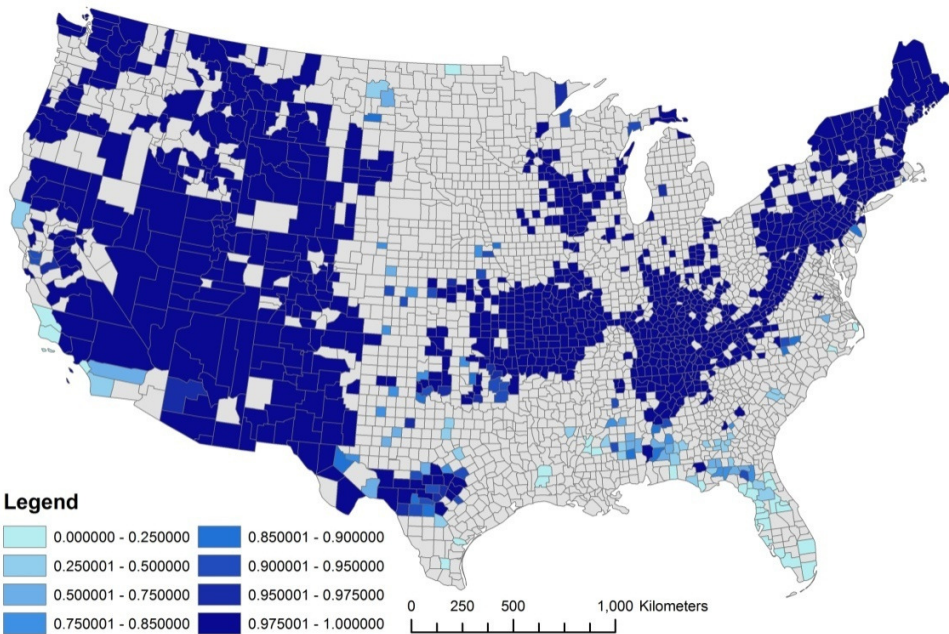
Supplementary Figure S36. Mean estimated year of infection, when infection (yellow-to-red scale) is predicted from simulations begun from currently infected counties (2010–2011; blue color scale) under the gravity_{caves+winter} model using the ML parameter set and climate data from SRES A1B Scenario. Grey counties did not have reported caves or WNS observations. The model predicts spread to most (94% P.I. 94%–95%) of the counties with caves in the contiguous United States within a century of the first infection, most within the next 20 years. Spread to the southeast is slow and to parts of the Midwest and southern California; longer time to infection in the Upper Midwest and New England may be due to edge effects (see Discussion).



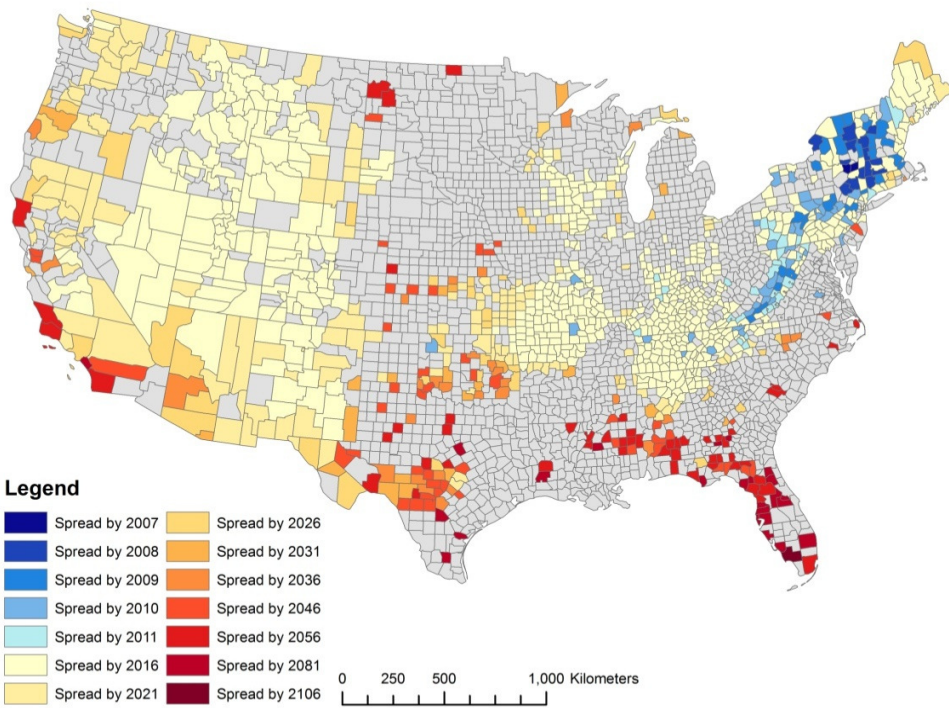
Supplementary Figure S37. The frequency of counties becoming infected by the winter of 2100–211 under the $\text{gravity}_{\text{caves}} + \text{winter}$ model using the ML parameter set and climate data from SRES A1B Scenario. Counties in southern Florida were not always reached, but most the remaining counties with caves are likely to be infected.



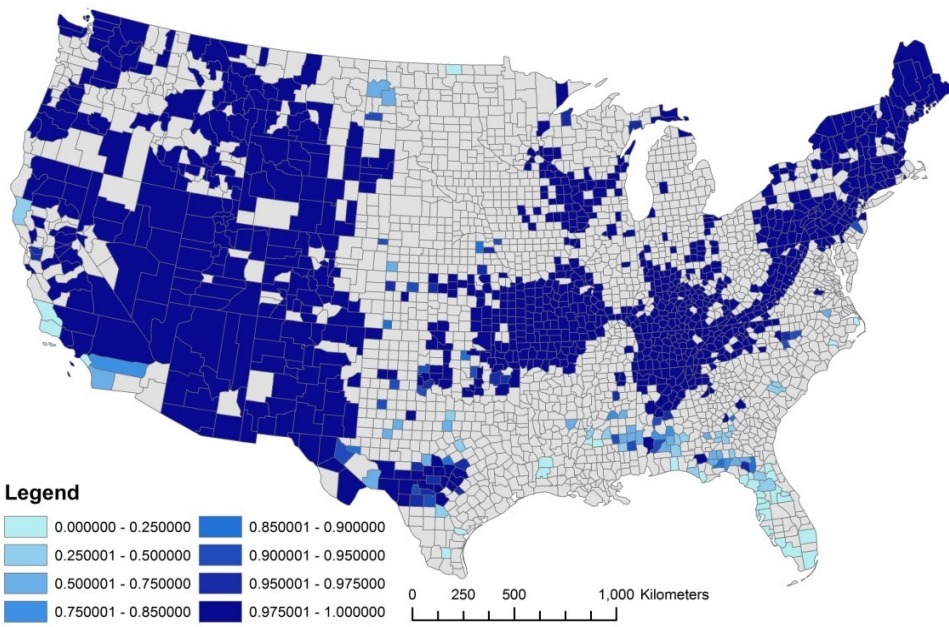
Supplementary Figure S38. Mean estimated year of infection, when infection (yellow-to-red scale) is predicted from simulations begun from currently infected counties (2010–2011; blue color scale) under the gravity_{caves+winter} model using the ML parameter set and climate data from SRES A2 Scenario. Grey counties did not have reported caves or WNS observations. The model predicts spread to most (94% P.I. 94%–95%) of the counties with caves in the contiguous United States within a century of the first infection, most within the next 20 years. Spread to the southeast is slow and to parts of the Midwest and southern California; longer time to infection in the Upper Midwest and New England may be due to edge effects (see Discussion).



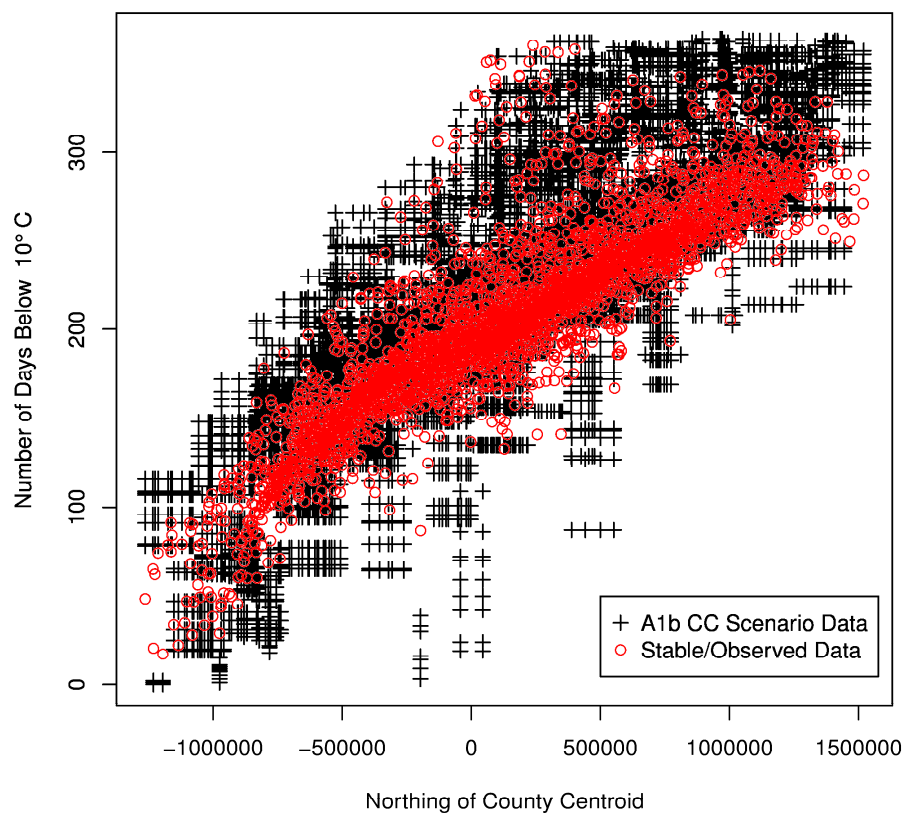
Supplementary Figure S39. The frequency of counties becoming infected by the winter of 2105–2106 under the gravity_{caves}+winter model using the ML parameter set and climate data from SRES A2 Scenario. Counties in southern Florida were not always reached, but most the remaining counties with caves are likely to be infected.



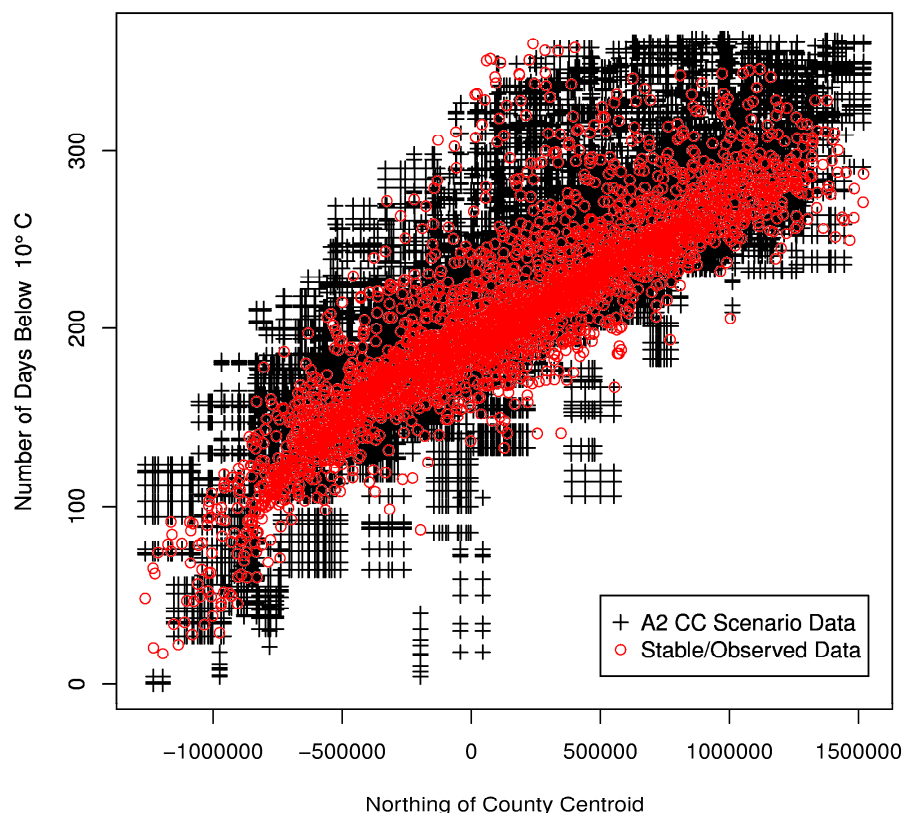
Supplementary Figure S40. Mean estimated year of infection, when infection (yellow-to-red scale) is predicted from simulations begun from currently infected counties (2010–2011; blue color scale) under the gravity_{caves+winter} model using the ML parameter set and climate data from SRES B1 Scenario. Grey counties did not have reported caves or WNS observations. The model predicts spread to most (95% P.I. 94%–96%) of the counties with caves in the contiguous United States within a century of the first infection, most within the next 20 years. Spread to the southeast is slow and to parts of the Midwest and southern California; longer time to infection in the Upper Midwest and New England may be due to edge effects (see Discussion).



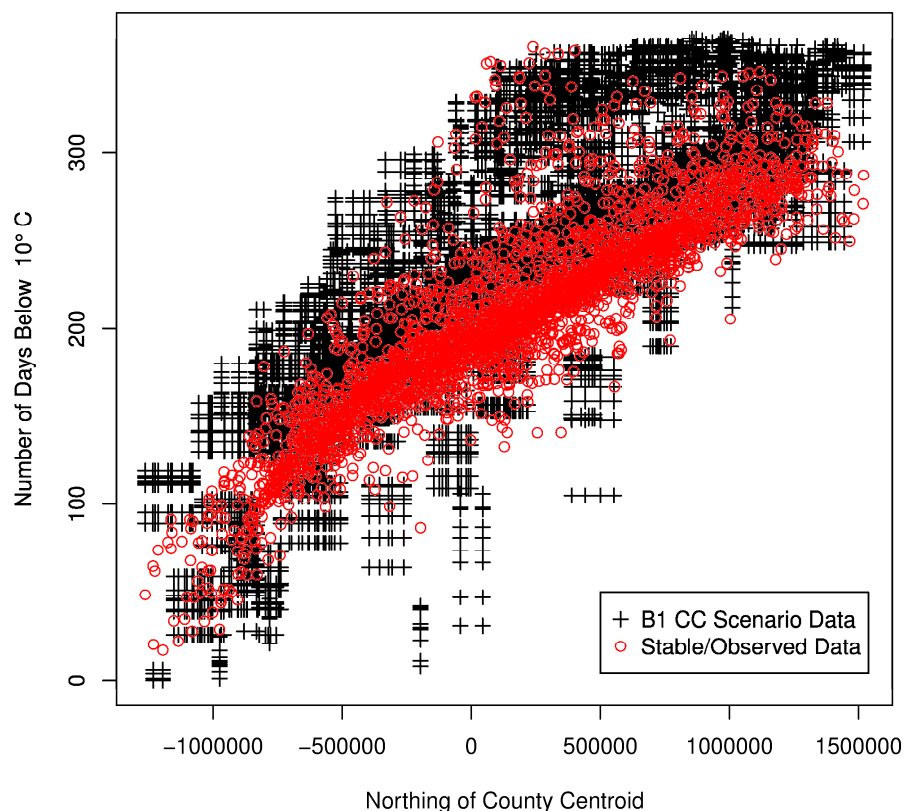
Supplementary Figure S41. The frequency of counties becoming infected by the winter of 2105–2106 under the gravity_{caves}+winter model using the ML parameter set and climate data from SRES B1 Scenario. Counties in southern Florida were not always reached, but most the remaining counties with caves are likely to be infected.



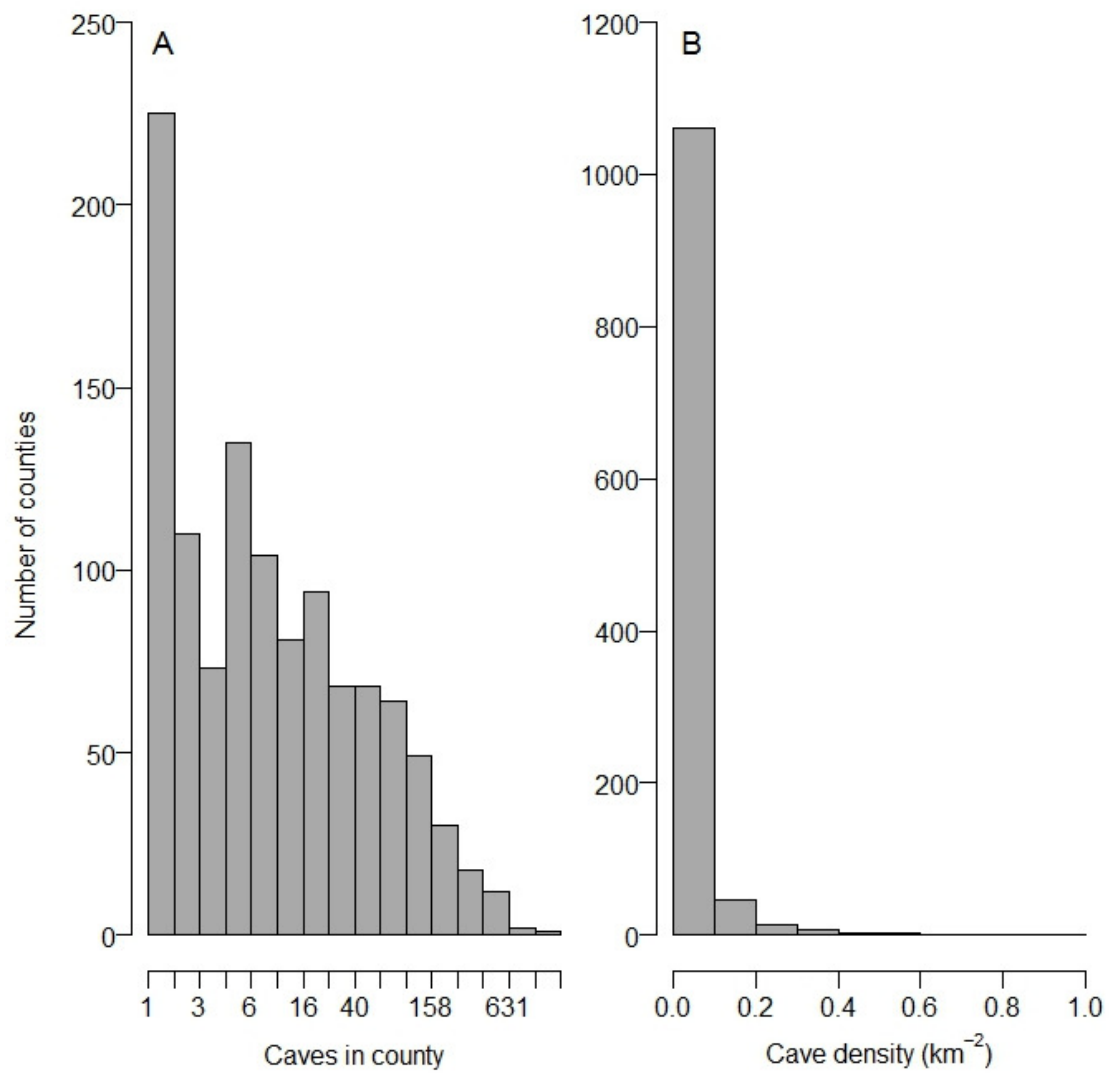
Supplementary Figure S42. Scatterplot of calculated winter length (number of days the minimum was below 10°C) and northing of the county centroid. Black crosses represent data from SRES A1B Scenario and open red circles represent observed data from 2006–2009.



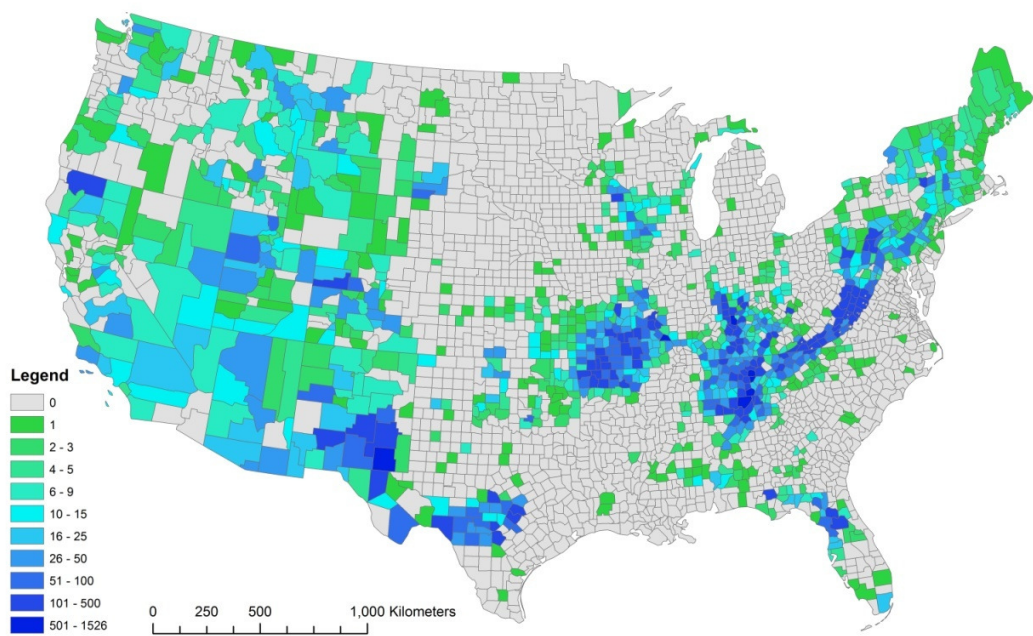
Supplementary Figure S43. Scatterplot of calculated winter length (number of days the minimum was below 10°C) and northing of the county centroid. Black crosses represent data from SRES A2 Scenario and open red circles represent observed data from 2006–2009.



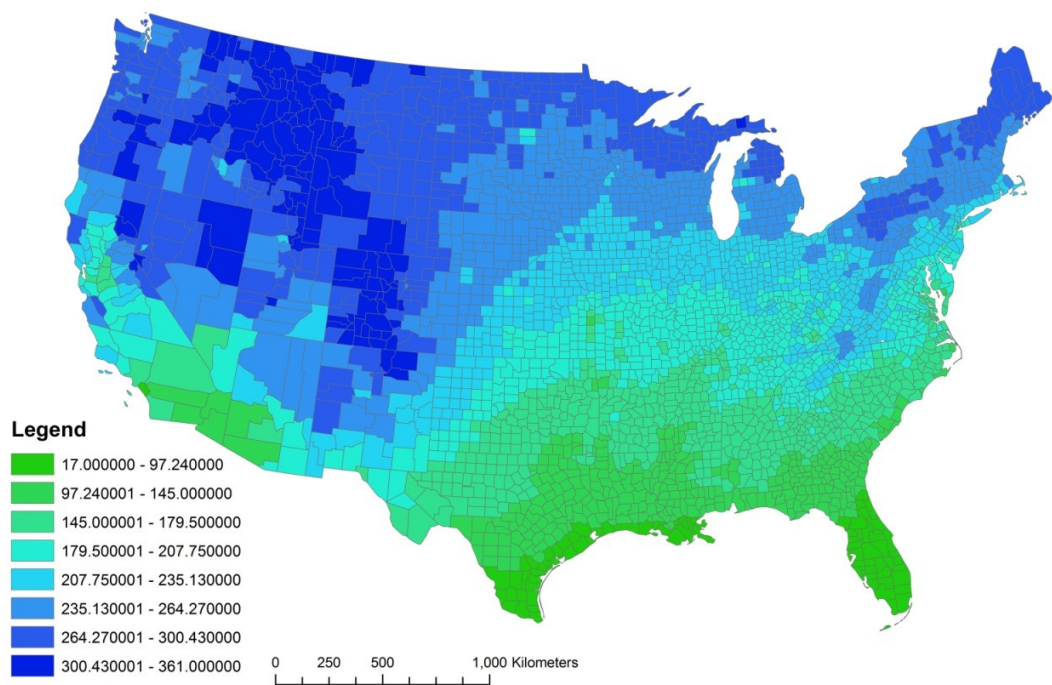
Supplementary Figure S44. Scatterplot of calculated winter length (number of days the minimum was below 10°C) and northing of the county centroid. Black crosses represent data from SRES B1 Scenario and open red circles represent observed data from 2006–2009.



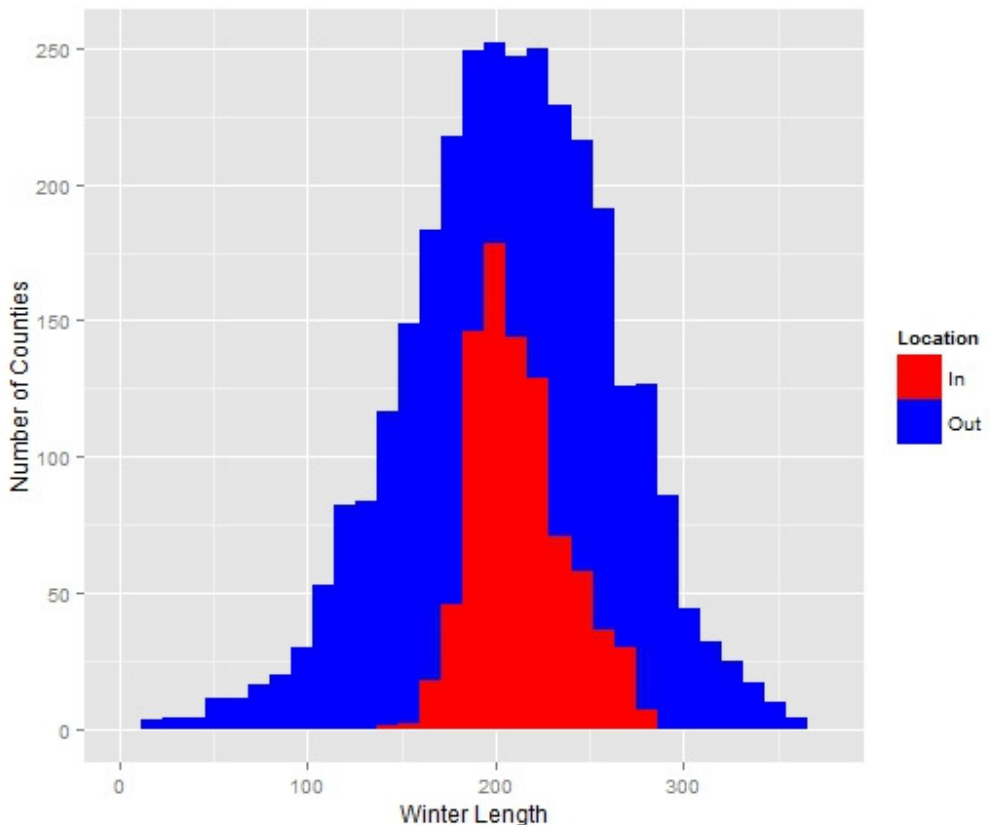
Supplementary Figure S45. Histograms of counties and caves in our dataset for the contiguous United States. The skew of the frequency of caves in counties (A) is less extreme than the density of caves (number of caves per km²; B).



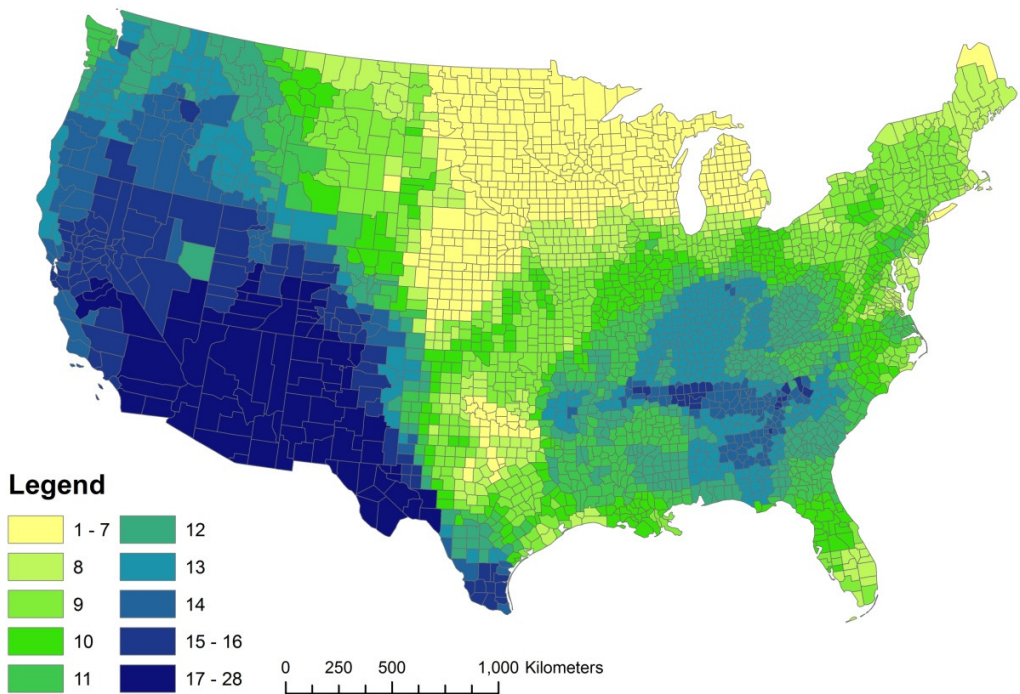
Supplementary Figure S46. The geographic distribution of the density of caves per county in our dataset. There are high density counties within the Appalachian Mountains and in the Ozarks, and lower values in the west.



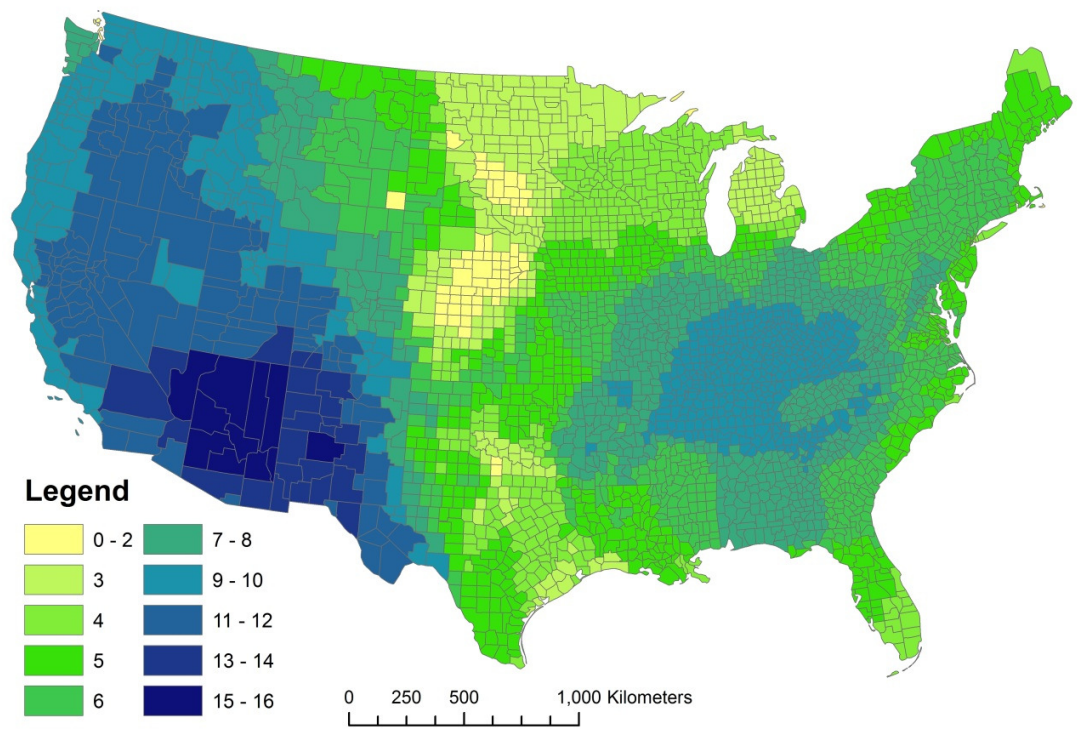
Supplementary Figure S47. The mean number of days in year with minimum temperature below 10°C from January 2006–December 2009.



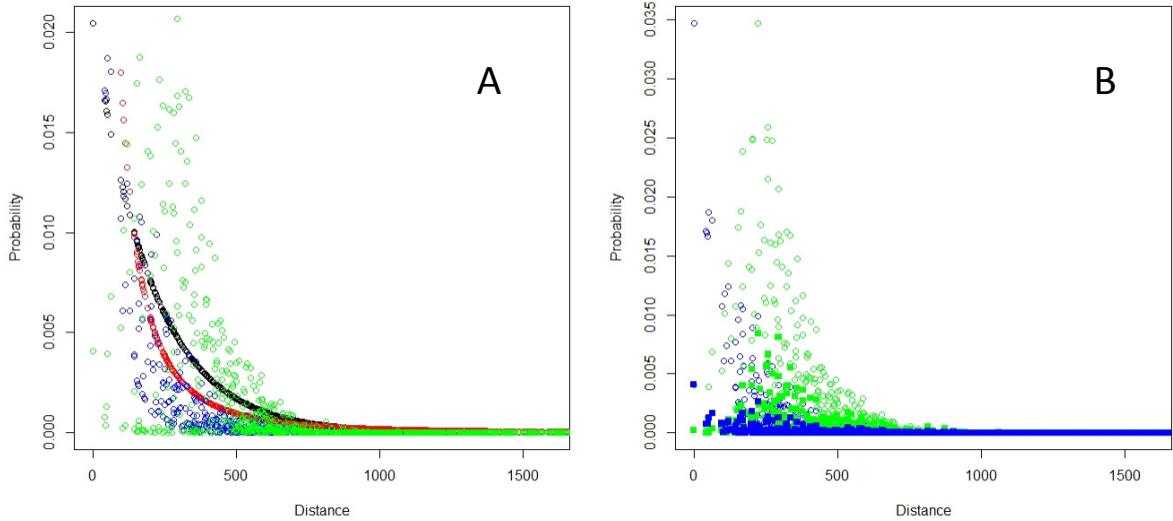
Supplementary Figure S48. A stacked histogram representing the count of counties in bins of various winter lengths for those within the convex hull of observed infected (red) and those outside (blue). The counties that are most likely to be influential in our analysis are centered within the overall distribution of winter lengths.



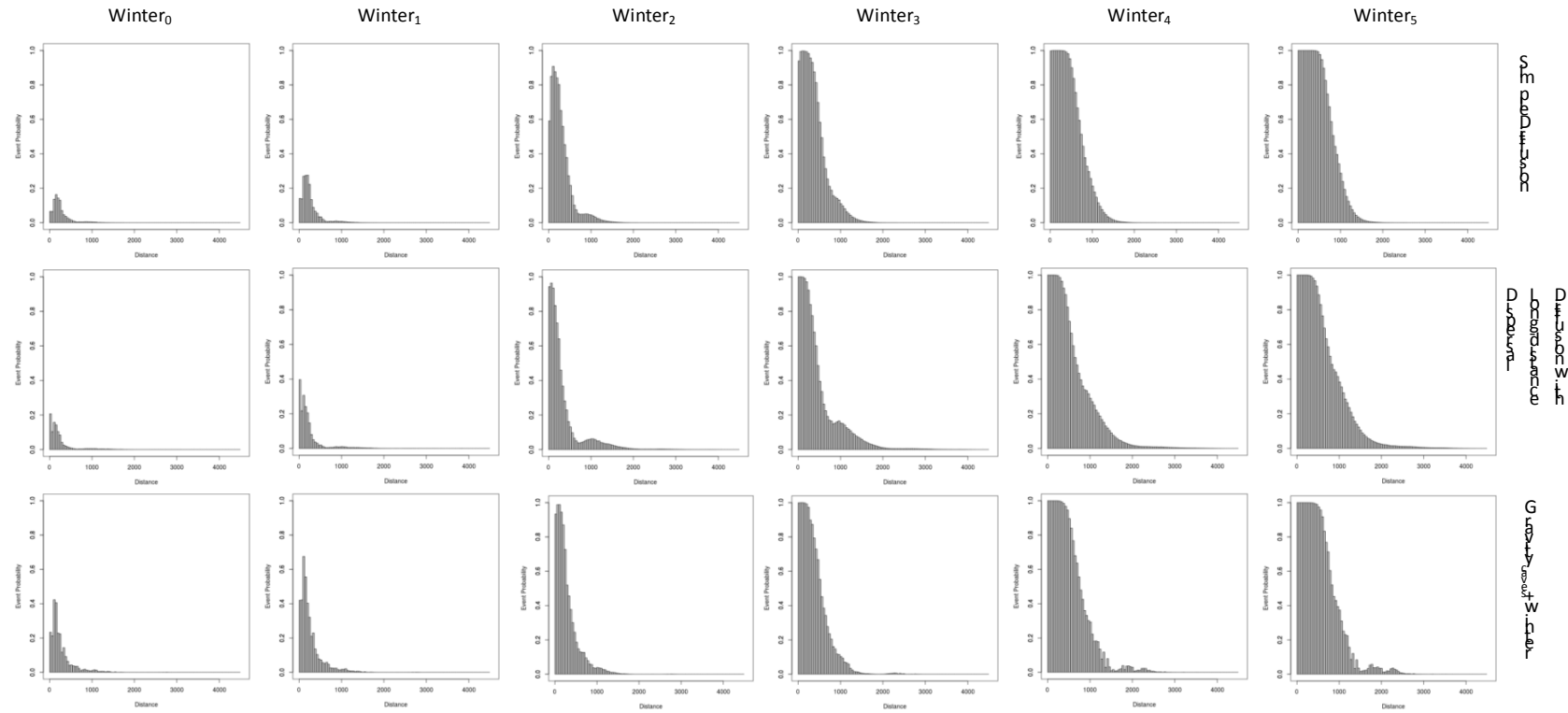
Supplementary Figure S49. Bat species richness by county in the contiguous United States as calculated from range maps.



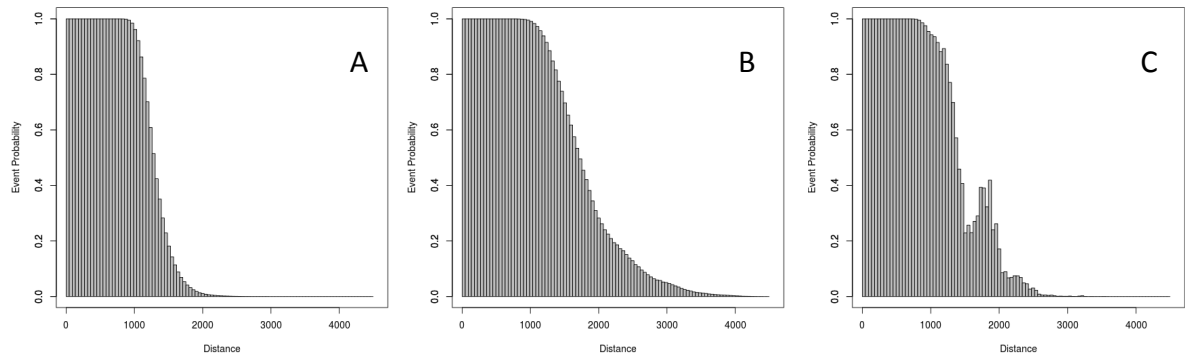
Supplementary Figure S50. Bat species richness of those species that hibernate by county in the contiguous United States as calculated from range maps.



Supplementary Figure S51. The decay with distance of the probability of spread from a single county. In A, the probabilities for the simple diffusion (black circles), diffusion with long-distance dispersal (red circles), and gravity_{caves} for two counties with different number of caves ($n_i=17$, blue circles; $n_i=1526$, green circles) are shown to be reduced with distance. In B, the probabilities from the gravity_{caves} kernels (circles) are compared to those for the gravity_{caves}+winter model (squares) to show the effect of the winter term.



Supplementary Figure S52. The change in event probability with distance for the successive years of spread for three of models that represent our hypothesized expectations of spread. In each set, a distinct peak of probabilities near 1000km appears due to the frequency of this distance within the full network of counties with caves. However, in the diffusive models, this bimodal pattern disappears after the fourth winter, whereas additional peaks in the fourth and fifth winter appear around 2000km for the gravity_{caves}+model. Both the diffusion with long-distance dispersal model and the gravity_{caves}+winter model have distributions with a “fat tail” that allows for long-distance transmission events.



Supplementary Figure S53. The decay in event probability with distance for the entire network of counties with caves under different models with the assumption that all nodes are infected. In A (simple diffusion), the decay occurs rapidly after 1000km, while in B (diffusions with long-distance dispersal) and C (gravity_{caves}+winter), the probability of an event is greater at larger distances (e.g. distances greater than 1500km), demonstrating the opportunity for long-distance dispersal events with these kernels.

Supplementary Table S1. Distance white-nose syndrome traveled in each of the 5 current years of spread

Winter	Mean Distance (km)	SD	Median Distance (km)	Max Distance (km)	Minimum Distance (km)	Number of New Counties
2006–2007	37.749	-	37.749	37.749	37.749	1
2007–2008	112.609	51.240	107.691	203.100	33.834	14
2008–2009	212.222	247.126	51.240	795.209	31.381	27
2009–2010	187.903	302.208	97.204	1568.940	29.960	39
2010–2011	71.062	71.008	47.661	307.473	26.734	30

Supplementary Table S2. ML parameters (β ; approximate 95% confidence limits^a) for the addition models of spread and goodness of fit to the observed data.

Hypothesis	f() ^b	Support ^c	β_0	β_1	β_2	β_3	NLL	AIC
Simple Diffusion + Winter	$\beta_0 + \beta_1 d_{ij} + \beta_2 \tau_i$	Caves	7.246 (-2.53–9.77)	0.004 (0.00–0.01)	-0.014 (-0.01–0.00)		387	780
Simple Diffusion + Northing	$\beta_0 + \beta_1 d_{ij} + \beta_2 \tau_i$	Caves	4.023	4.821	-0.0000002		395	796
Simple Diffusion + Caves	$\beta_0 + \beta_1 d_{ij} + \beta_2 n_i$	Caves	3.190 (2.91–3.47)	0.017 (0.01–0.02)	0.148 (0.12–0.18)		389	784
Simple Diffusion + Area	$\beta_0 + \beta_1 d_{ij} + \beta_2 a_i$	Caves	4.025 (3.71–4.34)	0.005 (0.004–0.006)	-0.0001 (-0.0002–0.0)		393	792
Simple Diffusion + Species Richness	$\beta_0 + \beta_1 d_{ij} + \beta_2 s_i$	Caves	3.204 (2.41–4.00)	0.005 (0.004–0.006)	0.074 (-0.01–0.16)		394	794
Simple Diffusion + Hibernating	$\beta_0 + \beta_1 d_{ij} + \beta_2 H_i$	Caves	3.818 (3.19–4.44)	0.005 (0.004–0.006)	0.008 (-0.08–0.10)		395	796
Diffusion with Long-Distance Dispersal + Winter	$\beta_0 + \beta_1 d_{ij}^{\beta_2} + \beta_3 \tau_i$	Caves	0.566 (-8.83–9.97)	2.280 (-3.62–8.19)	0.223 (-0.03–0.47)	-0.012 (-0.019–0.005)	378	764
Diffusion with Long-Distance Dispersal + Northing	$\beta_0 + \beta_1 d_{ij}^{\beta_2} + \beta_3 \tau_i$	Caves	-2.150	2.065	0.240	-0.0000001	384	776
Diffusion with Long-Distance Dispersal + Caves	$\beta_0 + \beta_1 d_{ij}^{\beta_2} + \beta_3 n_i$	Caves	-1.477 (-6.35–3.39)	1.670 (-1.15–4.49)	0.262 (0.08–0.44)	-0.002 (-0.003–0.001)	378	764
Diffusion with Long-Distance Dispersal + Area	$\beta_0 + \beta_1 d_{ij}^{\beta_2} + \beta_3 a_i$	Caves	-1.427 (-6.04–3.19)	1.655 (-0.97–4.28)	0.264 (0.10–0.43)	-0.00009 (-0.00015–0.00003)	383	774
Diffusion with Long-Distance Dispersal + Species Richness	$\beta_0 + \beta_1 d_{ij}^{\beta_2} + \beta_3 s_i$	Caves	-2.894 (-3.43–2.36)	2.195 (2.01–2.38)	0.231 (0.22–0.24)	0.058 (0.003–0.114)	384	776
Diffusion with Long-Distance Dispersal + Hibernating	$\beta_0 + \beta_1 d_{ij}^{\beta_2} + \beta_3 H_i$	Caves	-2.158 (-9.28–4.96)	2.063 (-2.33–6.45)	0.2398 (-0.02–0.46)	-0.004 (-0.13–0.12)	384	776
Gravity (Area) + Species Richness	$\beta_0 + \beta_1 \frac{d_{ij}}{(n_i n_j)^{\beta_2}} + \beta_3$	Caves	4.013 (3.37–4.65)	0.323 (0.24–0.40)	-0.026 (-0.10–0.04)	0.621 (-0.15–1.39)	388	784
Gravity (Area) + Hibernating	$\beta_0 + \beta_1 \frac{d_{ij}}{(n_i n_j)^{\beta_2}} + \beta_3$	Caves	4.38 (3.89–4.87)	0.844 (-0.11–1.80)	0.340 (0.27–0.41)	-0.107 (-0.18–0.03)	386	780
Gravity (Area) + Northing	$\beta_0 + \beta_1 \frac{d_{ij}}{(n_i n_j)^{\beta_2}} + \beta_3$	Caves	3.522	8.870	0.343	0.00003	387	782
Gravity (Area) + Winter	$\beta_0 + \beta_1 \frac{d_{ij}}{(n_i n_j)^{\beta_2}} + \beta_3$	Caves	5.898 (3.67–8.13)	0.092 (-0.21–0.40)	0.204 (-0.01–0.42)	-0.008 (-0.02–0.00)	386	780

^aThe approximate 95% confidence limits of the maximum likelihood parameters in multivariate parameter space, unless the covariance matrix is singular and, therefore, the bounds are not calculable simultaneously.

^bThe function from Eq. 1.

^cModels were fit to either the contiguous United States (All) or counties with caves in the contiguous United States (Caves)

Supplementary Table S3. Amount of deviation explained by additional parameters in the geographical restricted models representing our initial hypotheses of spread.

	Simple Diffusion	Diffusion with Long-distance Dispersal	Gravity _{caves}	Gravity _{caves} +Winter
Diffusion with Long-distance Dispersal	22*	-	-	-
Gravity _{area}	14*	-	-	-
Gravity _{caves}	36*	-	-	-
Gravity _{caves} + Species Richness	68*	46*	32*	-
Gravity _{caves} + Hibernating	58*	36*	22*	-
Gravity _{caves} + Northing	70*	48*	34*	-
Gravity _{caves} + Winter	96*	74*	60*	-
Gravity _{caves} + Winter + Species Richness	96*	74*	60*	0

*P-value < 0.0001

Supplementary Table S4. Results of simulations of select models that reflect our initial hypotheses of spread using the ML parameter sets.

Form	Diffusion with Long-Distance Dispersal													
	Simple Diffusion		All		Simple Diffusion		All		Diffusion with Long-Distance Dispersal		Gravity _{caves}			
Scale	All	2005–2006	2010–2011	All	2005–2006	2010–2011	Restricted	2005–2006	2010–2011	Restricted	2005–2006	2010–2011	Gravity _{caves} +Northing	Gravity _{caves} +Winter
Initial Winter of Infections	2005–2006	2010–2011	2005–2006	2010–2011	2005–2006	2010–2011	Restricted	2005–2006	2010–2011	Restricted	2005–2006	2010–2011	2005–2006	2010–2011
Expected Maximum Spread to New Counties (MS)	307	352	332	358	136	157	135	152	114	144	96	104	95	98
Winter of MS	2017–2018	2014–2015	2017–2018	2015–2016	2015–2014	2013–2016	2015–2014	2013–2016	2014–2015	2013–2014	2013–2014	2013–2014	2014–2015	2013–2014
Winter of Upper Limit MS	2016–2017	2014–2015	2017–2018	2015–2016	2014–2015	2013–2014	2014–2015	2013–2014	2013–2014	2013–2014	2013–2014	2013–2014	2013–2014	2013–2014
Winter of Lower Limit MS	2019–2020	2014–2015	2019–2020	2015–2016	2016–2017	2013–2014	2016–2017	2013–2014	2015–2016	2013–2014	2014–2015	2013–2014	2014–2015	2014–2015
Winter of Maximum Distance Spread (Mx)	2052–2053	2048–2049	2037–2038	2034–2035	2040–2041	2038–2039	2033–2034	2031–2032	2067–2068	2065–2066	2055–2056	2054–2055	2033–2034	2032–2033
Winter of Upper Limit Mx	2036–2037	2033–2034	2022–2023	2021–2022	2027–2028	2025–2026	2019–2020	2017–2018	2040–2041	2038–2039	2027–2028	2026–2027	2019–2020	2019–2019
Winter of Lower Limit Mx	2072–2073	2068–2069	2056–2057	2055–2056	2059–2058	2057–2058	2053–2054	2052–2053	2105–2106	2103–2104	2102–2103	2104–2105	2056–2056	2056–2057
Median Distance of Spread (Md)	1548.83	1548.83	1548.83	1548.83	1460.52	1460.52	1548.83	1460.52	1455.81	1455.81	1414.04	1415.11	1407.89	1407.92
Winter of Md	2092–2093	2088–2089	2078–2079	2075–2076	2027–2028	2060–2061	2033–2034	2055–2056	2103–2104	2101–2102	2105–2106	2105–2106	2104–2105	2105–2106
Winter of Upper Limit Md	2072–2073	2068–2069	2059–2060	2057–2058	2051–2052	2049–2050	2045–2046	2044–2045	2098–2099	2096–2097	2105–2106	2105–2106	2104–2105	2104–2105
Winter of Lower Limit Md	2097–2098	2093–2094	2090–2091	2088–2089	2089–2090	2087–2088	2079–2080	2076–2077	2105–2106	2104–2105	2105–2106	2105–2106	2104–2105	2104–2105
Maximum Convex Hull Area (CHA)	9929633	9929633	9929633	9929633	9673843	9673843	9673843	9673843	9673843	9673843	8908811	8910667	8684123	8684608
Winter of CHA	2075–2076	2071–2072	2059–2060	2056–2057	2056–2057	2054–2055	2048–2049	2047–2048	2101–2102	2099–2100	2105–2106	2105–2106	2105–2106	2105–2106
Winter of Upper Limit CHA	2056–2057	2053–2054	2043–2044	2041–2042	2082–2083	2082–2083	2040–2041	2034–2041	2083–2084	2082–2083	2104–2105	2105–2106	2103–2104	2105–2106
Winter of Lower Limit CHA	2103–2014	2102–2103	2105–2106	2105–2106	2103–2014	2104–20105	2105–2106	2099–2100	2105–2106	2105–2106	2105–2106	2105–2106	2104–2105	2104–20105
Counties in which Winter of Infection Underestimated Median Proportion Counties Infected expected in 2105–2106 (PCI)	86	-	92	-	29	-	29	-	10	-	10	-	6	-
Upper Limit PCI	1.00	1.00	1.00	1.00	1.00	1.00	1.00	1.00	0.99	0.99	0.95	0.95	0.93	0.93
Lower Limit PCI	1.00	1.00	1.00	1.00	1.00	1.00	1.00	1.00	0.99	0.99	0.94	0.94	0.92	0.92

Supplementary Table S5. Results of simulations of models that reflect our initial hypotheses of spread using the SU parameter sets.

Form	Simple Diffusion		Diffusion with Long-Distance Dispersal		Simple Diffusion		Diffusion with Long-Distance Dispersal		Gravity _{caves}		Gravity _{caves+Northing}		Gravity _{caves+Winter}	
	All 2005– 2006	All 2010– 2011	All 2005– 2006	All 2010– 2011	Restricted 2005– 2006	Restricted 2010– 2011	Restricted 2005– 2006	Restricted 2010– 2011	Restricted 2005– 2006	Restricted 2010– 2011	Restricted 2005– 2006	Restricted 2010– 2011	Restricted 2005– 2006	Restricted 2010– 2011
Initial Winter of Infections														
Maximum Spread to New Counties (MS)	301	354	37	342	132	157	15	332	115	148	97	107	96	102
Winter of MS	2017– 2018	2014– 2015	2014– 2015	2011– 2012	2014– 2015	2013– 2014	2011– 2012	2011– 2012	2013– 2014	2012– 2013	2013– 2014	2013– 2014	2013– 2014	2013– 2014
Winter of Upper Limit MS	2016– 2017	2014– 2015	2006– 2007	2011– 2012	2013– 2014	2013– 2014	2006– 2007	2011– 2012	2012– 2013	2012– 2013	2012– 2013	2012– 2013	2012– 2013	2013– 2014
Winter of Lower Limit MS	2019– 2020	2015– 2016	2006– 2007	2011– 2012	2016– 2017	2013– 2014	2006– 2007	2011– 2012	2015– 2016	2013– 2014	2014– 2015	2013– 2014	2014– 2015	2014– 2015
Maximum Distance (km) of Spread (Mx)	4053.97	4053.97	4053.97	4053.97	4053.97	4053.97	3133.02	4053.97	4053.97	4053.97	4053.97	4053.97	4053.97	4053.97
Winter of Mx	2052– 5053	2048– 2049	2014– 2015	2016– 2017	2040– 2041	2038– 2039	2010– 2011	2013– 2014	2064– 2065	2062– 2063	2052– 2053	2051– 2052	2031– 2032	2031– 2032
Winter of Upper Limit Mx	2034– 2035	2031– 2032	2006– 2007	2011– 2012	2025– 2026	2024– 2025	2006– 2007	2011– 2012	2033– 2034	2032– 2033	2023– 2024	2022– 2023	2017– 2018	2017– 2018
Winter of Lower Limit Mx	2076– 2077	2071– 2072	2047– 2048	2044– 2045	2061– 2062	2058– 2059	2031– 2032	2042– 2043	2092– 2093	2089– 2090	2091– 2092	2090– 2091	2059– 2060	2058– 2059
Medain Distance (km) of Spread (Md)	1548.83	1548.83	1548.83	1548.83	1460.52	1460.52	795.33	1460.52	1455.81	1456.85	1415.36	1415.36	1407.99	1407.99
Winter of Md	2092– 2093	2089– 2090	2021– 2022	2023– 2024	2062– 2063	2060– 2061	2009– 2010	2016– 2017	2101– 2102	2104– 2105	2105– 2106	2104– 2105	2104– 2105	2104– 2105
Winter of Upper Limit Md	2065– 2066	2062– 2063	2006– 2007	2011– 2012	2046– 2047	2045– 2046	2014– 2015	2011– 2012	2085– 2086	2084– 2085	2101– 2086	2100– 2086	2102– 2103	2102– 2103
Winter of Lower Limit Md	2098– 2099	2100– 2101	2096– 2097	2094– 2095	2096– 2097	2094– 2095	2017– 2018	2064– 2065	2105– 2106	2105– 2106	2104– 2105	2104– 2105	2104– 2105	2104– 2105
Maximum Convex Hull Area (km ² , CHA)	9929633	9929633	9929633	9929633	9673843	9673843	9673843	9673843	9655708	9657113	8906111	8908811	8681775	8683063
Winter of CHA	2077– 2078	2073– 2074	2054– 2055	2051– 2052	2060– 2061	2057– 2058	2048– 2049	2045– 2046	2100– 2101	2098– 2099	2102– 2103	2103– 2104	2104– 2105	2105– 2106
Winter of Upper Limit CHA	2052– 2053	2050– 2051	2006– 2007	2011– 2012	2039– 2040	2083– 2084	2007– 2008	2064– 2065	2061– 2062	2060– 2061	2085– 2086	2086– 2087	2101– 2102	2102– 2103
Winter of Lower Limit CHA	2104– 2105	2105– 2106	2105– 2106	2105– 2106	2104– 2105	2096– 2097	2095– 2096	2095– 2096	2103– 2104	2013– 2104	2104– 2105	2104– 2105	2105– 2106	2105– 2106
Counties in which Winter of Infection Underestimated	84		0		28		0		7		7		5	
Median Proportion Counties Infected expected in 2105–2106 (PCI)	1.00	1.00	1.00	1.00	1.00	1.00	1.00	1.00	0.99	1.00	0.95	0.95	0.93	0.93
Upper Limit PCI	1.00	1.00	1.00	1.00	1.00	1.00	1.00	1.00	1.00	1.00	0.99	0.99	0.97	0.97
Lower Limit PCI	1.00	1.00	1.00	1.00	1.00	1.00	1.00	1.00	0.97	0.98	0.90	0.90	0.90	0.90

Supplementary Table S6. Results of simulations under three climate scenarios using the gravity_{caves}+winter model.

Climate Scenario	A1b		A2		B1	
Parameter Set	ML 2010–2011	SU 2010–2011	ML 2010–2011	SU 2010–2011	ML 2010–2011	SU 2010–2011
Initial Winter of Infections						
Maximum Spread to New Counties (MS)	193	197	207	214	184	185
Winter of MS	2013–2014	2013–2014	2012–2013	2012–2013	2013–2014	2013–2014
Winter of Upper Limit MS	2013–2014	2013–2014	2012–2013	2012–2013	2013–2014	2012–2013
Winter of Lower Limit MS	2013–2014	2013–2014	2012–2013	2012–2013	2013–2014	2013–2014
Maximum Distance (km) of Spread (Mx)	4037.09	4037.09	4037.09	4037.09	4037.09	4037.09
Winter of Mx	2020–2021	2020–2021	2020–2021	2020–2021	2023–2024	2023–2024
Winter of Upper Limit Mx	2018–2019	2017–2018	2018–2019	2018–2019	2019–2020	2018–2019
Winter of Lower Limit Mx	2045–2046	2046–2047	2056–2057	2056–2057	2043–2044	2044–2045
Median Distance (km) of Spread (Md)	1414.04	1415.11	1415.11	1415.36	1422.41	1422.41
Winter of Md	2097–2098	2097–2098	2097–2098	2097–2098	2100–2101	2098–2099
Winter of Upper Limit Md	2100–2101	2096–2097	2097–2098	2091–2092	2099–2100	2100–2101
Winter of Lower Limit Md	2099–2100	2100–2101	2099–2100	2097–2098	2099–2100	2098–2099
Maximum Convex Hull Area (km ² , CHA)	8650999	8657680	8654086	8659585	8678411	8683156
Winter of CHA	2100–2101	2100–2101	2099–2100	2100–2101	2100–2101	2099–2100
Winter of Upper Limit CHA	2100–2101	2096–2097	2099–2100	2099–2100	2099–2100	2100–2101
Winter of Lower Limit CHA	2100–2101	2096–2097	2098–2099	2095–2096	2099–2100	2099–2100
Median Proportion Counties Infected expected in 2105–2106 (PCI)	0.94	0.94	0.94	0.95	0.95	0.95
Upper Limit PCI	0.95	0.97	0.95	0.97	0.96	0.98
Lower Limit PCI	0.94	0.92	0.94	0.92	0.94	0.93

Supplementary Methods

Habitat Data

Bats that hibernate use a variety of natural and anthropogenic features as hibernacula^{43–44,25} where conditions for growth of the *G. destructans* may be met⁷. To estimate the geographic distribution of available sites we searched for cave and mine locations across the epidemic region. Distribution of caves in the United States has been documented⁴⁵ and we acquired a partial record from the lead author (D. Culver) listing the number of documented caves in each county within 36 of the contiguous United States. Data were missing for 12 states (Kansas, Louisiana, Maine, Mississippi, Nebraska, North Carolina, North Dakota, Ohio, South Carolina, South Dakota, Wisconsin, and Wyoming). Moore⁴⁶ provided the relevant cave density data for Mississippi. To complete the coverage of states, we magnified Fig. 1 of Culver et al.⁴⁵ and estimated the number of caves within each county. In some cases, points that represent cave locations in this figure overlapped at high cave densities, and so the number of caves within the county were likely underestimated. In such counties we could accurately estimate cave numbers to a maximum of ~15 caves. Supplementary Fig. S45 shows the relative frequency of caves within the 1,117 United States counties documented to contain caves and the relative frequency of cave densities within these counties. Supplementary Fig. S46 shows the geographic distribution of our cave data set. A comparison of these data to WNS occurrence records revealed 22 WNS occurrence records were in counties lacking documented caves; in most cases (21 of 22) these records could be shown to be associated with mines. Because mine type, status (active and inactive), and distribution data were not available, we accounted for each of these WNS occurrences by adding a single “cave” in the identified county to our database. Matching data in terms of quality and breadth were not available for Canada, and so we restricted analyses to the contiguous United States.

Because *G. destructans* is known to be cryophilic², pathogenesis is temperature dependent³², and cause of death in lethal cases is believed to be starvation and physiological stress^{5,47–48}, we hypothesized that winter temperatures would be a key determinant of transmission and spread. Accordingly, we developed a nationwide map of winter duration as follows. Daily minimum temperature data from all United States weather stations active between January 2006–December 2009 were acquired from NOAA's National Climate Data Center (NCDC; <http://www.ncdc.noaa.gov/oa/ncdc.html>). For each station, we calculated the mean number of days per year where the minimum recorded temperature was less than 10° C. These results were interpolated with anisotropic ordinary kriging (12 lags of 382 km, spherical model, major axis = 4336346.447869585 m, minor axis = 2420321.056366793 m, direction = 82.35806369781494°, sill = 6623.3240469201 m) using ArcGIS (ver. 9.3, www.esri.com) to create a consistently calculated, smooth representation of winter duration across the contiguous United States (Supplementary Fig. S47). Finally, the mean of grid cells within each county was calculated.

WNS infects multiple species. Because theory predicts that host species composition can influence the prevalence and occurrence of infection³ we sought to investigate if bat species richness and composition influenced spread. To estimate bat richness by county, we acquired geographic range data from NatureServe (www.natureserve.com) for the 46 species most likely to occur in any part of the contiguous United States at some point in the year. We generated an indicator matrix of presence and absence of each species (columns) for each county (rows) and the sum of across rows was considered species richness, *S*, for each county. The geographic

variation in distribution is evident where higher richness is found near the southern Appalachians and throughout the west (Supplementary Fig. S49). We also summed across rows to determine the number of bat species that hibernate, H_i , that may occur in a given county during the year. (Supplementary Fig. S50).

Climate change scenario data

We used simulated climate data from three of the standard International Panel on Climate Change (IPCC) scenarios (SRES B1, least change in climate; A1B, intermediate change; and A2, most change) to project how climate change could alter the spread of WNS in the contiguous United States. Because the length of winter variable used in the model was calculated as the number of days the minimum temperature fell below 10°C, climate simulations providing daily data on minimum temperature represent the most direct way to estimate the length of winter as included in the model. The CM2.0 global circulation model from Geophysical Fluid Dynamics Laboratory (NOAA) provided simulated daily minimum temperature ('tas_min') data for the period 2001-2100 (http://nomads.gfdl.noaa.gov/CM2.X/CM2.0/available_data.html). Other widely used global circulation models did not have these data easily available for the entire period, as the IPCC only required reporting daily values for specific 20 year periods. Values in the simulated data represent grid cells 2° latitude by 2.5° longitude, so forecasted data are at a much coarser scale than the weather station data used to estimate the covariate in the model. We extracted the daily minimum temperature for all grid cells in the United States and summed the number of days where the minimum temperature fell below 10°C in each calendar year. Subsequently, winter length in each county in each year was assigned as the value of the grid cell that overlapped the county centroid.

Calculation of Probabilities

The probability that the infection spreads from county j to county i under a given dispersal kernel $f(\cdot)$ is given by

$$p_{ij} = \frac{1}{1 + e^f}.$$

The probability that the infection does not spread from county j to county i , is

$$1 - p_{ij} = 1 - \frac{1}{1 + e^f}.$$

Through re-arrangement and combination we find the equation,

$$1 - \frac{1}{1 + e^f} = \frac{1 + e^f - 1}{1 + e^f} = \frac{e^f}{1 + e^f}.$$

Dividing the numerator and the denominator of the expression above by e^f , we obtain

$$1 - p_{ij} = \frac{1}{1 + e^{-f}},$$

which we denote by \tilde{p}_{ij} . Eq. S4 is Eq. 1 in the main text.

For the epidemiological model which describes the force of infection¹⁹, the probability that a county i is infected by county j was estimated directly, and there was no need for the logit transformation.

Additional models

To further examine potential explanatory models of spread we fit a series of additional

models that added a single covariate with the simple diffusion, diffusion with long-distance dispersal, and the area gravity kernels. Available covariates for these diffusion kernels included winter length, northing, cave density, area of the county, total bat species richness, and number of hibernating bat species; for area gravity kernel we tested winter length, total bat species richness, and number of hibernating bat species as covariates (Supplementary Eqs. S2–S7, S9–S14, S16–S19). In some cases, the additional covariate improved performance compared to the kernel alone, but in all cases, models did not fit the observed data better than our preferred model (Supplementary Table S2).

Dispersal Kernel Equations

Supplementary Equation S1. Simple Diffusion

The probability of county j not infecting county i in a given time step where the parameters are set as the background infection rate (β_0) and the distance between the two counties (d_{ij}) multiplied by a coefficient (β_1). Coefficients were fit to the data simultaneously using maximum likelihood.

$$\tilde{p}_{ij} = \frac{1}{1 + e^{-(\beta_0 + \beta_1 d_{ij})}}$$

Supplementary Equation S2. Simple Diffusion + Winter

The probability of county j not infecting county i in a given time step where the parameters are set as the background infection rate (β_0) and the distance between the two counties (d_{ij}) multiplied by a coefficient (β_1). The effect of winter (see Materials and Methods), τ_i , was varied based on a coefficient, β_2 . Coefficients were fit to the data simultaneously using maximum likelihood.

$$\tilde{p}_{ij} = \frac{1}{1 + e^{-(\beta_0 + \beta_1 d_{ij} + \beta_2 \tau_i)}}$$

Supplementary Equation S3. Simple Diffusion + Northing

The probability of county j not infecting county i in a given time step where the parameters are set as the background infection rate (β_0) and the distance between the two counties (d_{ij}) multiplied by a coefficient (β_1). The effect of geographic position (see Materials and Methods), τ_i , was varied based on a coefficient, β_2 . Coefficients were fit to the data simultaneously using maximum likelihood.

$$\tilde{p}_{ij} = \frac{1}{1 + e^{-(\beta_0 + \beta_1 d_{ij} + \beta_2 \tau_i)}}$$

Supplementary Equation S4. Simple Diffusion + Caves

The probability of county j not infecting county i in a given time step where the parameters are set as the background infection rate (β_0) and the distance between the two counties (d_{ij}) multiplied by a coefficient (β_1). The effect of caves, n_i , was varied based on a coefficient, β_2 . Coefficients were fit to the data simultaneously using maximum likelihood.

$$\tilde{p}_{ij} = \frac{1}{1 + e^{-(\beta_0 + \beta_1 d_{ij} + \beta_2 n_i)}}$$

Supplementary Equation S5. Simple Diffusion + Area

The probability of county j not infecting county i in a given time step where the parameters are set as the background infection rate (β_0) and the distance between the two counties (d_{ij}) multiplied by a coefficient (β_1). The effect of area of the county, a_i , was varied based on a coefficient, β_2 . Coefficients were fit to the data simultaneously using maximum likelihood.

$$\tilde{p}_{ij} = \frac{1}{1 + e^{-(\beta_0 + \beta_1 d_{ij} + \beta_2 a_i)}}$$

Supplementary Equation S6. Simple Diffusion + Species Richness

The probability of county j not infecting county i in a given time step where the parameters are set as the background infection rate (β_0) and the distance between the two counties (d_{ij}) multiplied by a coefficient (β_1). The effect of species richness, S_i , was varied based on a coefficient, β_2 . Coefficients were fit to the data simultaneously using maximum likelihood.

$$\tilde{p}_{ij} = \frac{1}{1 + e^{-(\beta_0 + \beta_1 d_{ij} + \beta_2 S_i)}}$$

Supplementary Equation S7. Simple Diffusion + Hibernating

The probability of county j not infecting county i in a given time step where the parameters are set as the background infection rate (β_0) and the distance between the two counties (d_{ij}) multiplied by a coefficient (β_1). The effect of species richness of those bats that hibernate, H_i , was varied based on a coefficient, β_2 . Coefficients were fit to the data simultaneously using maximum likelihood.

$$\tilde{p}_{ij} = \frac{1}{1 + e^{-(\beta_0 + \beta_1 d_{ij} + \beta_2 H_i)}}$$

Supplementary Equation S8. Simple Diffusion with Long-distance Dispersal

The probability of county j not infecting county i in a given time step where the parameters are set as the background infection rate (β_0) and the distance between the two counties (d_{ij}) multiplied by a coefficient (β_1). The effect of distance was varied based on an exponential coefficient, β_2 . Coefficients were fit to the data simultaneously using maximum likelihood.

$$\tilde{p}_{ij} = \frac{1}{1 + e^{-(\beta_0 + \beta_1 d_{ij}^{\beta_2})}}$$

Supplementary Equation S9. Simple Diffusion with Long-distance Dispersal + Winter

The probability of county j not infecting county i in a given time step where the parameters are set as the background infection rate (β_0) and the distance between the two counties (d_{ij}) multiplied by a coefficient (β_1). The effect of distance was varied based on an exponential coefficient, β_2 ; the effect of winter (see Materials and Methods), τ_i , was varied based on a coefficient, β_3 . Coefficients were fit to the data simultaneously using maximum likelihood.

$$\tilde{p}_{ij} = \frac{1}{1 + e^{-(\beta_0 + \beta_1 d_{ij}^{\beta_2} + \beta_3 \tau_i)}}$$

Supplementary Equation S10. Simple Diffusion with Long-distance Dispersal + Northing
The probability of county j not infecting county i in a given time step where the parameters are set as the background infection rate (β_0) and the distance between the two counties (d_{ij}) multiplied by a coefficient (β_1). The effect of distance was varied based on an exponential coefficient, β_2 ; the effect of geographic position (see Materials and Methods), τ_i , was varied based on a coefficient, β_3 . Coefficients were fit to the data simultaneously using maximum likelihood.

$$\tilde{p}_{ij} = \frac{1}{1 + e^{-(\beta_0 + \beta_1 d_{ij}^{\beta_2} + \beta_3 \tau_i)}}$$

Supplementary Equation S11. Simple Diffusion with Long-distance Dispersal + Caves
The probability of county j not infecting county i in a given time step where the parameters are set as the background infection rate (β_0) and the distance between the two counties (d_{ij}) multiplied by a coefficient (β_1). The effect of distance was varied based on an exponential coefficient, β_2 ; the effect of caves, n_i , was varied based on a coefficient, β_3 . Coefficients were fit to the data simultaneously using maximum likelihood.

$$\tilde{p}_{ij} = \frac{1}{1 + e^{-(\beta_0 + \beta_1 d_{ij}^{\beta_2} + \beta_3 n_i)}}$$

Supplementary Equation S12. Simple Diffusion with Long-distance Dispersal + Area
The probability of county j not infecting county i in a given time step where the parameters are set as the background infection rate (β_0) and the distance between the two counties (d_{ij}) multiplied by a coefficient (β_1). The effect of distance was varied based on an exponential coefficient, β_2 ; the effect of area of the county, a_i , was varied based on a coefficient, β_3 . Coefficients were fit to the data simultaneously using maximum likelihood.

$$\tilde{p}_{ij} = \frac{1}{1 + e^{-(\beta_0 + \beta_1 d_{ij}^{\beta_2} + \beta_3 a_i)}}$$

Supplementary Equation S13. Simple Diffusion with Long-distance Dispersal + Species Richness
The probability of county j not infecting county i in a given time step where the parameters are set as the background infection rate (β_0) and the distance between the two counties (d_{ij}) multiplied by a coefficient (β_1). The effect of distance was varied based on an exponential coefficient, β_2 ; the effect of species richness, S_i , was varied based on a coefficient, β_3 . Coefficients were fit to the data simultaneously using maximum likelihood.

$$\tilde{p}_{ij} = \frac{1}{1 + e^{-(\beta_0 + \beta_1 d_{ij}^{\beta_2} + \beta_3 S_i)}}$$

Supplementary Equation S14. Simple Diffusion with Long-distance Dispersal + Hibernating
The probability of county j not infecting county i in a given time step where the parameters are set as the background infection rate (β_0) and the distance between the two counties (d_{ij}) multiplied by a coefficient (β_1). The effect of distance was varied based on an exponential coefficient, β_2 ; the effect of species richness of those bats that hibernate, H_i , was varied based on a coefficient, β_3 . Coefficients were fit to the data simultaneously using maximum likelihood.

$$\tilde{p}_{ij} = \frac{1}{1 + e^{-(\beta_0 + \beta_1 d_{ij}^{\beta_2} + \beta_3 H_i)}}$$

Supplementary Equation S15. Gravity_{area}

The probability of county j not infecting county i in a given time step where the parameters are set as the background infection rate (β_0) and the distance between the two counties (d_{ij}) divided by the product of county area, the gravity term, multiplied by a coefficient (β_1). The magnitude of the gravity term was fixed based on an exponential coefficient, β_2 . Coefficients were fit to the data simultaneously using maximum likelihood.

$$\tilde{p}_{ij} = \frac{1}{1 + e^{-\left(\beta_0 + \beta_1 \frac{d_{ij}}{(a_i a_j)^{\beta_2}}\right)}}$$

Supplementary Equation S16. Gravity_{area}+Species Richness

The probability of county j not infecting county i in a given time step where the parameters are set as the background infection rate (β_0) and the distance between the two counties (d_{ij}) divided by the product of cave densities, the gravity term, multiplied by a coefficient (β_1). The magnitude of the gravity term was fixed based on an exponential coefficient, β_2 . The effect of the species richness, S_i , was fixed by the coefficient β_3 . Coefficients were fit to the data simultaneously using maximum likelihood.

$$\tilde{p}_{ij} = \frac{1}{1 + e^{-\left(\beta_0 + \beta_1 \frac{d_{ij}}{(n_i n_j)^{\beta_2}} + \beta_3 S_i\right)}}$$

Supplementary Equation S17. Gravity_{area}+Hibernating

The probability of county j not infecting county i in a given time step where the parameters are set as the background infection rate (β_0) and the distance between the two counties (d_{ij}) divided by the product of cave densities, the gravity term, multiplied by a coefficient (β_1). The magnitude of the gravity term was fixed based on an exponential coefficient, β_2 . The effect of the species richness of those bats that hibernate, H_i , was fixed by the coefficient β_3 . Coefficients were fit to the data simultaneously using maximum likelihood.

$$\tilde{p}_{ij} = \frac{1}{1 + e^{-\left(\beta_0 + \beta_1 \frac{d_{ij}}{(n_i n_j)^{\beta_2}} + \beta_3 H_i\right)}}$$

Supplementary Equation S18. Gravity_{area}+Winter

The probability of county j not infecting county i in a given time step where the parameters are set as the background infection rate (β_0) and the distance between the two counties (d_{ij}) divided by the product of cave densities, the gravity term, multiplied by a coefficient (β_1). The magnitude of the gravity term was fixed based on an exponential coefficient, β_2 . The effect of the length of winter (Materials and Methods), τ_i , was fixed by the coefficient β_3 . Coefficients were fit to the data simultaneously using maximum likelihood.

$$\tilde{p}_{ij} = \frac{1}{1 + e^{-\left(\beta_0 + \beta_1 \frac{d_{ij}}{(n_i n_j)^{\beta_2}} + \beta_3 \tau_i\right)}}$$

Supplementary Equation S19. Gravity_{area}+Northing

The probability of county j not infecting county i in a given time step where the parameters are set as the background infection rate (β_0) and the distance between the two counties (d_{ij}) divided by the product of cave densities, the gravity term, multiplied by a coefficient (β_1). The magnitude of the gravity term was fixed based on an exponential coefficient, β_2 . The effect of the geographic position (Materials and Methods), τ_i , was fixed by the coefficient β_3 . Coefficients were fit to the data simultaneously using maximum likelihood.

$$\tilde{p}_{ij} = \frac{1}{1 + e^{-\left(\beta_0 + \beta_1 \frac{d_{ij}}{(n_i n_j)^{\beta_2}} + \beta_3 \tau_i\right)}}$$

Supplementary Equation S20. Gravity_{caves}

The probability of county j not infecting county i in a given time step where the parameters are set as the background infection rate (β_0) and the distance between the two counties (d_{ij}) divided by the product of cave densities, the gravity term, multiplied by a coefficient (β_1). The magnitude of the gravity term was fixed based on an exponential coefficient, β_2 . Coefficients were fit to the data simultaneously using maximum likelihood.

$$\tilde{p}_{ij} = \frac{1}{1 + e^{-\left(\beta_0 + \beta_1 \frac{d_{ij}}{(n_i n_j)^{\beta_2}}\right)}}$$

Supplementary Equation S21. Gravity_{caves}+Species Richness

The probability of county j not infecting county i in a given time step where the parameters are set as the background infection rate (β_0) and the distance between the two counties (d_{ij}) divided by the product of cave densities, the gravity term, multiplied by a coefficient (β_1). The magnitude of the gravity term was fixed based on an exponential coefficient, β_2 . The effect of the species richness, S_i , was fixed by the coefficient β_3 . Coefficients were fit to the data simultaneously using maximum likelihood.

$$\tilde{p}_{ij} = \frac{1}{1 + e^{-\left(\beta_0 + \beta_1 \frac{d_{ij}}{(n_i n_j)^{\beta_2}} + \beta_3 S_i\right)}}$$

Supplementary Equation S22. Gravity_{caves}+Hibernating

The probability of county j not infecting county i in a given time step where the parameters are set as the background infection rate (β_0) and the distance between the two counties (d_{ij}) divided by the product of cave densities, the gravity term, multiplied by a coefficient (β_1). The magnitude of the gravity term was fixed based on an exponential coefficient, β_2 . The effect of the species richness of those bats that hibernate, H_i , was fixed by the coefficient β_3 . Coefficients were fit to the data simultaneously using maximum likelihood.

$$\tilde{p}_{ij} = \frac{1}{1 + e^{-\left(\beta_0 + \beta_1 \frac{d_{ij}}{(n_i n_j)^{\beta_2}} + \beta_3 H_i\right)}}$$

Supplementary Equation S23. Gravity_{caves}+Winter

The probability of county j not infecting county i in a given time step where the parameters are set as the background infection rate (β_0) and the distance between the two counties (d_{ij}) divided by the product of cave densities, the gravity term, multiplied by a coefficient (β_1). The magnitude of the gravity term was fixed based on an exponential coefficient, β_2 . The effect of the length of winter (Materials and Methods), τ_i , was fixed by the coefficient β_3 . Coefficients were fit to the data simultaneously using maximum likelihood.

$$\tilde{p}_{ij} = \frac{1}{1 + e^{-\left(\beta_0 + \beta_1 \frac{d_{ij}}{(n_i n_j)^{\beta_2}} + \beta_3 \tau_i\right)}}$$

Supplementary Equation S24. Gravity_{caves}+Northing

The probability of county j not infecting county i in a given time step where the parameters are set as the background infection rate (β_0) and the distance between the two counties (d_{ij}) divided by the product of cave densities, the gravity term, multiplied by a coefficient (β_1). The magnitude of the gravity term was fixed based on an exponential coefficient, β_2 . The effect of the geographic position (Materials and Methods), τ_i , was fixed by the coefficient β_3 . Coefficients were fit to the data simultaneously using maximum likelihood.

$$\tilde{p}_{ij} = \frac{1}{1 + e^{-\left(\beta_0 + \beta_1 \frac{d_{ij}}{(n_i n_j)^{\beta_2}} + \beta_3 \tau_i\right)}}$$

Supplementary Equation S25. Gravity_{caves}+Winter+Species Richness

The probability of county j not infecting county i in a given time step where the parameters are set as the background infection rate (β_0) and the distance between the two counties (d_{ij}) divided by the product of cave densities, the gravity term, multiplied by a coefficient (β_1). The magnitude of the gravity term was fixed based on an exponential coefficient, β_2 . The effect of the length of winter (Materials and Methods), τ_i , was fixed by the coefficient β_3 . The effect of species richness, S_i , was fixed by the coefficient β_4 . Coefficients were fit to the data simultaneously using maximum likelihood.

$$\tilde{p}_{ij} = \frac{1}{1 + e^{-\left(\beta_0 + \beta_1 \frac{d_{ij}}{(n_i n_j)^{\beta_2}} + \beta_3 \tau_i + \beta_4 S_i\right)}}$$

Supplementary Equation S26. Force of Infection

The probability of county j infecting county i in a given time step was fit by a complex model reflecting the normalized force of infection based on cave density, winter length and distance. The first parameter was set as the background infection rate (β_0) and the effect of the winter term τ_i , was fixed by the coefficient β_1 . The effect of the number of caves in county i , n_i , was fixed by the linear coefficient β_2 and the exponential coefficient β_3 . This effect was multiplied by the sum across all counties j , of the number of caves in county j , n_j , divided by the distance between the two counties, d_{ij} . The effects of the n_j was fixed by the exponential coefficient β_4 ; likewise the effect of d_{ij} was fixed by exponential coefficient β_6 . In the normalization term, the number of caves in county j , n_j , was divided by the distance between counties, d_{ij} , fixed by an exponential coefficient β_5 ; this value was fixed by an exponential coefficient β_5 and summed across all counties j . Coefficients were fit to the data simultaneously using maximum likelihood

$$\tilde{p}_{ij} = \beta_0 + \beta_1 \tau_i + \frac{\beta_2 n_i^{\beta_3} \times \sum_j \left[\left(\frac{n_j^{\beta_4}}{d_{ij}^{\beta_6}} \right) \right]}{\left(\sum_j \left(\frac{n_j}{d_{ij}^{\beta_5}} \right) \right)^{\beta_5}}$$

Supplementary Equation S27. Radiation Model

The probability of county j infecting county i in a given time step was fit by a complex model²⁰ based on cave density, winter length and distance. The first parameter was set as the background infection rate (β_0) and the effects of the winter term τ_i , and the distance between counties, d_{ij} , were fixed by the coefficients β_1 and β_2 , respectively. The radiation term includes the density of caves within counties, n_i and n_j , as well as a term representing the number of caves within a radius equal to d_{ij} from the county j . The effect of this term was estimated by β_3 . Coefficients were fit to the data simultaneously using maximum likelihood

$$p_{ij} = 1 - e^{\left\{ \beta_0 + \beta_1 \tau_i + \beta_2 d_{ij} + \beta_3 \frac{n_j^2 n_i}{(n_j c_{ij})(n_j + n_i + c_{ij})} \right\}}$$

β_n —parameter

d_{ij} —distance between counties i and j

n_i —number of caves in county i

n_j —number of caves in county j

a_i —area of county i

a_j —area of county j

τ_i —covariate (either northing or length of winter)

S_i —covariate for species richness

H_i —covariate for species richness of hibernating bats

c_{ij} – estimated “circle mass”

\tilde{p}_{ij} – probability that county_i is not infected by county_j

p_{ij} – probability that county_i is infected by county_j

Parameter estimation

For each model, we created a network where each county centroid was a node with a binary state variable to represent the infected/uninfected status and edges weighted by the requisite dispersal function. The maximum likelihood (ML) parameters for each model were obtained using the Nelder-Mead (NM) algorithm (function `optim` in the R package `stats`⁴⁰), beginning the search from an arbitrary parameter set that returned a finite value. Once `optim` returned a parameter set, we initiated another search under the NM algorithm starting where the previous run ended; this was repeated until the same parameter set was returned from subsequent runs. We further performed a Simulated Annealing (SANN) search from this parameter set to confirm that other global optima did not exist. In each case, SANN did not find a novel parameter set, and so we infer that returned parameters represent the maximum likelihood estimate. To assign confidence intervals to our ML parameters we solved for the 95th equi-coordinate quantile through the function `qmvnorm` (package: `mvtnorm`⁴¹) and solved

$$\frac{q \times \sqrt{\text{diag}(\mathbf{A})}}{k}$$

where q is the equi-coordinate quantile⁴⁹ and \mathbf{A} is the variance-covariance matrix obtained by inverting the hessian matrix at the maximum likelihood estimate, which we obtained numerically using the R package `numDeriv`⁴².

Simulation of spread

To compare the spatial characteristics of each model and observed data, stochastic spread was simulated from Schoharie County (time t_0) for 100 years, excluding models that included the species richness term because these were redundant. For successive time steps, we calculated the probability of infection of counties for the given network, model, and ML parameter set and conducted a Bernoulli trial to see if that county became infected in the next time step. The stochastic update formula for the status of county i was

$$x_i(t+1) \sim \text{Bernoulli} \left(1 - \exp \left[\sum_j \ln(1 - p_{ij}) \right] \right)$$

where x is the infection status of the county i of interest that was uninfected in time t , j represents the vector of infected counties and p_{ij} is the result of the spatial kernel. This process was iterated using the infection status at time (t) to calculate the probabilities of infection and simulate the infection status at time ($t+1$), where t is the year in the series.

Supplementary References

43. Fenton, M. B. Population studies of *Myotis lucifugus* (Chiroptera: Vespertilionidae) in Ontario (Royal Ontario Museum Publications in Life Science, Toronto Canada). (1970)
44. Altringham, J. D. *Bats: Biology and Behavior* (Oxford Univer Press, New York, New York). (1996)
45. Culver, D. C., Hobbs III, H. H., Christman, M. C. & Master, L. L. Distribution map of caves and cave animals in the United States J Cave Karst Studies 61, 139–140. (1999)
46. Moore, C. M. Dissolution caves of Mississippi. Master's Thesis, Mississippi State University. (2006)
47. Cryan, P. M., Meteyer, C., Boyles, J. G. & Blehert, D. S. Wing pathology of White-nose Syndrome in bats suggests life-threatening disruption of physiology. BMC Biology 8, 135. (2010)
48. Storm, J. J. & Boyles J. G. Body temperature and body mass of hibernating little brown bats *Myotis lucifugus* in hibernacula affected by White-nose Syndrome. Acta Theriol 56, 123–127. (2010)
49. Munzel, U. & Tamhane, A. C. Nonparametric multiple comparisons in repeated measures designs for data with ties. Biometrical J 44, 762–779. (2002)